

Synthesis and Characterization of Magnetic Nanoparticles (Co, FeCo, CoFe₂O₄, SmCo, Nd₂Fe₁₄B) and Their Nanocomposites

(자성체 나노입자 (Co, FeCo,
CoFe₂O₄, SmCo, Nd₂Fe₁₄B) 및
나노복합재료 합성 및 특성 연구)



Soo-Ja Shin

A thesis submitted in partial fulfillment of the requirements for the
degree of

Master of Science

in Department of Chemistry, The Graduate School,
Pukyong National University

February, 2006


Synthesis and Characterization of Magnetic Nanoparticles
(Co, FeCo, CoFe₂O₄, SmCo, Nd₂Fe₁₄B) and Their
Nanocomposites

A Dissertation
by
Soo Ja Shin

Approved by :


(Chairman) : Kum Sho Hwang


(Member) : Sung Doo Moon


(Member) : Young Soo Kang

February, 2006

Contents

| | |
|---|-----------|
| 1. Introduction | 1 |
| 2. Experimentals | 4 |
| 2-1. Background | 4 |
| 2-1-1. Introduction of nanotechnology..... | 4 |
| 2-1-2. Basic of ferromagnetism..... | 8 |
| 2-1-3. Nanostructured magnetic material..... | 9 |
| 2-1-4. Application of magnetic material..... | 10 |
| 2-1-5. Exchange coupled hard/soft magnet..... | 12 |
| 2-1-6. Synthetic method of nanosized-magnetic materials..... | 14 |
| 2-1-6-1. Polyol process..... | 14 |
| 2-1-6-2. Co-precipitation route..... | 15 |
| 2-2. Materials and method | 17 |
| 2-2-1. Preparation of Co nanoparticle by polyol method..... | 17 |
| 2-2-1-1. Preparation of Co nanoparticle..... | 17 |
| 2-2-1-2. Preparation of Co nanoparticle according to different precursors and size control..... | 18 |
| 2-2-2. Preparation of Co nanoparticle by new solventless thermal decomposition..... | 19 |
| 2-2-3. Preparation of Co nanoparticle by co-precipitation route..... | 21 |
| 2-2-4. Preparation of FeCo nanoparticle by polyol method..... | 22 |
| 2-2-4-1. Preparation of FeCo nanoparticle by polyol method..... | 22 |
| 2-2-5. Preparation of FeCo nanoparticle by co-precipitation route..... | 24 |

| | |
|--|-----------|
| 2-2-5-1. Preparation of FeCo nanoparticle by coprecipitation route..... | 24 |
| 2-2-5-2. Preparation of FeCo nanoparticle according to different precursors..... | 25 |
| 2-2-6. Preparation of CoFe_2O_4 nanoparticle by polyol method..... | 26 |
| 2-2-7. Preparation of SmCo nanoparticle by new solvetless thermal decomposition..... | 27 |
| 2-2-8. Preparation of $\text{Nd}_2\text{Fe}_{14}\text{B}$ alloy by ball milling..... | 29 |
| 2-2-9. Preparation of $\text{Nd}_2\text{Fe}_{14}\text{B}/\text{Co}$ nanocomposites by colloidal process..... | 30 |
| 2-3. Apparatus | 31 |
| 3. Results and discussion | 33 |
| 3-1. Preparation of Co nanoparticles..... | 33 |
| 3-1-1. Charecterization of Co nanoparticle prepared by polyol method..... | 33 |
| 3-1-1-1. X-ray powder diffraction (XRD)..... | 33 |
| 3-1-1-2. Field emission scanning electron microscopy (FE-SEM)..... | 35 |
| 3-1-1-3. Transmission electron microscopy (TEM)..... | 37 |
| 3-1-1-4. Energy dispersive X-ray spectrometer (EDS)..... | 39 |
| 3-1-1-5. Vibrating sample magnetometer (VSM)..... | 39 |
| 3-1-2. Characterization of Co nanoparticle prepared by co-precipitation route..... | 42 |
| 3-1-2-1. Transmission electron microscopy (TEM)..... | 42 |
| 3-1-2-2. X-ray powder diffraction (XRD)..... | 42 |
| 3-1-2-3. Electron probe X-ray micro analyzer (EPMA)..... | 43 |
| 3-1-2-4. Superconducting quantum interference device (SQUID)..... | 44 |
| 3-1-3. Charecterization of Co nanoparticle prepared by new | |

| | |
|--|-----------|
| solventless thermal decomposition..... | 45 |
| 3-1-3-1. Thermogravimetric analysis (TGA)..... | 45 |
| 3-1-3-2. Transmission electron microscopy (TEM)..... | 46 |
| 3-1-3-3. X-ray powder diffraction (XRD)..... | 47 |
| 3-1-3-4. Field emission scanning electron microscopy (FE-SEM)..... | 48 |
| 3-1-3-5. Energy dispersive X-ray spectrometer (EDS)..... | 49 |
| 3-1-3-6. Vibrating sample magnetometer (VSM)..... | 49 |
| 3-2. Preparation of FeCo nanoparticles..... | 50 |
| 3-2-1. Charecterization of FeCo nanoparticle prepared by co-precipitation route..... | 50 |
| 3-2-1-1. Transmission electron microscopy (TEM)..... | 50 |
| 3-2-1-2. Field emission scanning electron microscopy (FE-SEM)..... | 52 |
| 3-2-1-3. X-ray powder diffraction (XRD)..... | 54 |
| 3-2-1-4. Electron probe X-ray micro analyzer (EPMA)..... | 55 |
| 3-2-1-5. Vibrating sample magnetometer (VSM) | 58 |
| 3-2-2. Charecterization of FeCo nanoparticle prepared by polyol method..... | 61 |
| 3-2-2-1. Transmission electron microscopy (TEM)..... | 61 |
| 3-2-2-2. Field emission scanning electron microscopy (FE-SEM)..... | 63 |
| 3-2-2-3. X-ray powder diffraction (XRD)..... | 64 |
| 3-2-2-4. Energy dispersive X-ray spectrometer (EDS)..... | 65 |
| 3-2-2-5. Vibrating sample magnetometer (VSM) | 66 |
| 3-3. Preparation of CoFe₂O₄ nanoparticle..... | 66 |
| 3-3-1. Charecterization of CoFe ₂ O ₄ nanoparticle prepared by polyol method..... | 66 |
| 3-3-1-1. X-ray powder diffraction (XRD)..... | 67 |

| | |
|--|-----------|
| 3-3-1-2. Transmission electron microscopy (TEM)..... | 67 |
| 3-3-1-3. Energy dispersive X-ray spectrometer (EDS)..... | 69 |
| 3-3-1-4. Field emission scanning electron microscopy (FE-SEM)..... | 69 |
| 3-3-1-5. Superconducting quantum interference device (SQUID)..... | 70 |
| 3-4. Preparation of SmCo nanoparticles..... | 71 |
| 3-4-1. Preparation of SmCo nanoparticle prepared by new solventless thermal decomposition..... | 71 |
| 3-4-1-1. Thermogravimetric analysis (TGA)..... | 71 |
| 3-4-1-2. Transmission electron microscopy (TEM)..... | 72 |
| 3-4-1-3. X-ray powder diffraction (XRD)..... | 73 |
| 3-4-1-4. Field emission scanning electron microscopy (FE-SEM)..... | 74 |
| 3-4-1-5. Energy dispersive X-ray spectrometer (EDS)..... | 77 |
| 3-4-1-6. Vibrating sample magnetometer (VSM)..... | 78 |
| 3-5. Preparation of Nd₂Fe₁₄B/Co nanocomposites..... | 81 |
| 3-5-1. Preparation of Nd ₂ Fe ₁₄ B/Co nanocomposites by colloidal process..... | 81 |
| 3-5-1-1. X-ray powder diffraction (XRD)..... | 81 |
| 3-5-1-2. Electron probe X-ray micro analyzer (EPMA)..... | 82 |
| 3-5-1-3. Field emission scanning electron microscopy (FE-SEM)..... | 83 |
| 3-5-1-4. Vibrating sample magnetometer (VSM)..... | 84 |
| 4. Conclusion | 86 |
| 5. References | 87 |
| 6. Korean abstract | 92 |

Synthesis and Characterization of Magnetic Nanoparticles (Co, FeCo, CoFe₂O₄, SmCo, Nd₂Fe₁₄B) and Their Nanocomposites.

Soo Ja Shin

Department of Chemistry, Graduate School,
Pukyong National University

Abstract

In this research, the magnetic nanoparticles (Co, FeCo, CoFe₂O₄) were prepared by thermal decomposition and chemical reduction process. The Co and SmCo nanoparticles were synthesized with solventless thermal decomposition method by using a pyrex tube. And the core shell type of Nd₂Fe₁₄B/Co nanocomposite was prepared by colloidal process. As is usual with the previous study, their magnetic properties was compared with bulk magnetic materials. The values of M_s and coercivity for nanoparticles was also obtained from the ratio of their components. The size and shape were investigated with transmission electron microscopy and high resolution TEM images. The lattice spacing were investigated with high resolution TEM and the ratio of components with energy dispersive X-ray spectrometer (EDS). The decomposition of the complex was analyzed with thermogravimetric analysis (TGA) and the crystallization process was studied with X-ray powder diffraction (XRD). The morphology of the particle was characterized by field emission scanning electron microscope (FE-SEM). The magnetic properties were confirmed by superconducting quantum interference device (SQUID) and vibrating sample magnetometer (VSM).

1. Introduction

For many years, magnetic material nanoparticles have been investigated because of their unique properties compared with bulk material and continuous broadening of the area of application of new magnetic material¹⁻². Fine ferromagnetic metal particles for high density recording material, precious metals or copper particles for conductive inks and pastes used in the electronic industry, cobalt powder used in cemented carbide industry to make hard materials by metallurgy³⁻⁴. Several synthetic techniques have been applied to synthesize magnetic metal nanoparticles, including thermal decomposition⁵, metal evaporation⁶⁻⁷, sonochemical method⁸, reduction of metal salts by borohydride derivatives⁹⁻¹⁰, co-precipitation using microwave system¹¹ and chemical vapor condensation¹². Many studies on nanoparticles have focused on the synthesis of uniform spherical forms and the control of their particle size^{5,8,13-15}. In the chemical synthesis method, the control of size for nanoparticle is very important part¹⁶⁻¹⁷.

The polyol method¹⁸⁻¹⁹, that is known for providing monodisperse fine metal particles²⁰⁻²¹, afforded us the opportunity to synthesize ferromagnetic metal particles smaller than 2 μm and to investigate their dynamic properties. The polyol method is used to control the particle size and the nanoparticle is nucleated in high boiling point of polyol such as ethylene glycol, trimethylene glycol²².

The chemical reduction²³⁻²⁴ of transition metal ions by use of borohydride derivatives in the aqueous solution has been studied. The chemical coprecipitation method²⁵⁻²⁶ offers many advantages which are simple processes and room temperature as the reaction condition. And the control of size for the nanoparticle is a very important part. Chemically

coprecipitated compounds result in fine particle size of powder²⁷.

In this study, we report on the Co and FeCo-based soft magnetic nanoparticle materials that have received renewed interest since they exhibit high saturation magnetization (M_s)²⁸⁻²⁹. One can obtain the metal powder either by carrying out on amorphous powder obtained by reduction of Co^{2+} and Fe^{2+} cations with NaBH_4 from homogeneous solutions provided that this reaction can be conducted under kinetically controlled conditions³⁰⁻³¹ or from the general method of synthesis that is the following: an inorganic metallic compound or salt is dispersed in a liquid polyol³²⁻³⁴. Ethylene glycol is mainly used. The suspension is then stirred and heated to a given temperature, until complete reduction of the compound is complete. The metal is then recovered as a finely divided powder by centrifugation or filtration. This paper describes magnetic and structural properties of nano-sized FeCo particles by polyol process and coprecipitation method³⁵.

SmCo and Co magnetic nanoparticles were synthesized by a new solventless synthesis by metal-oleate complex thermolysis under low pressure. The magnetic properties of SmCo nanoparticle were compared according to the ratio of Sm to Co component. This thesis describes magnetic and structural properties of nano-sized SmCo and Co nanoparticles.

Nanocomposites of magnetically hard and soft phases have a substantial potential for application of permanent magnets, since their remanence could be higher than those in isotropic single-phase magnetically hard materials.³⁶ Remanence enhancement originates from the exchange coupling of magnetic moments across interfaces between the magnetically hard and soft phases, because the exchange coupling could turn the moments of the magnetically soft phase to rotate toward an average direction of the nearest neighboring magnetically hard phases. It has been demonstrated on several

occasions^{37,38} that the crystallite size of the phases, in particular, that of the soft phase, is important for realizing the remanence enhancement and determining the maximum energy product of the nanocomposite magnets. Much effort has been made to optimize the magnetic properties, by using various preparation methods, such as, mechanical alloying, melt spinning or sputtering³⁹⁻⁴², or element substitution^{43, 44}. In this study, the core shell type of Nd₂Fe₁₄B/Co nanocomposite was prepared by colloidal process. And their magnetic properties were compared according to the wt% of Co to Nd₂Fe₁₄B.

2. Experimentals

2-1. Background

2-1-1. Introduction of nanotechnology

Nanotechnology⁴⁵ deals with small structures or small-sized materials. The typical dimension spans from subnanometer to several hundred nanometers. A nanometer (nm) is one billionth of a meter, or 10^{-9} m. Figure 2-10 gives a partial list of zero-dimensional nanostructures with their typical ranges of dimension. One nanometer is approximately the length equivalent to 10 hydrogen or 5 silicon atoms in a line. Small features permit more functionality in a given space, but nanotechnology is not only a simple continuation of miniaturization from micron meter scale down to nanometer scale. Materials in the micrometer scale mostly exhibit physical properties the same as that of bulk form; however, materials in the nanometer scale may exhibit physical properties distinctively different from that of bulk. Materials in this size range exhibit some remarkable specific properties; a transition from atoms or molecules to bulk form takes place in the size range. For example, crystals in the nanometer scale have a low melting point (the difference can be as large as 1000 °C) and reduced lattice constants, since the number of surface atoms or ions and the surface energy plays a significant role in the thermal stability. Crystal structures stable at elevated temperatures are stable at much lower temperatures in nanometer sizes, so ferroelectrics and ferromagnetics may lose their ferroelectricity and ferromagnetism when the materials are shrunk to the nanometer scale. Bulk semiconductors become

insulators when the characteristic dimension is sufficiently small (in a couple of nanometers). Although bulk gold does not exhibit catalytic properties, Au nanocrystal demonstrates to be an excellent low temperature catalyst.

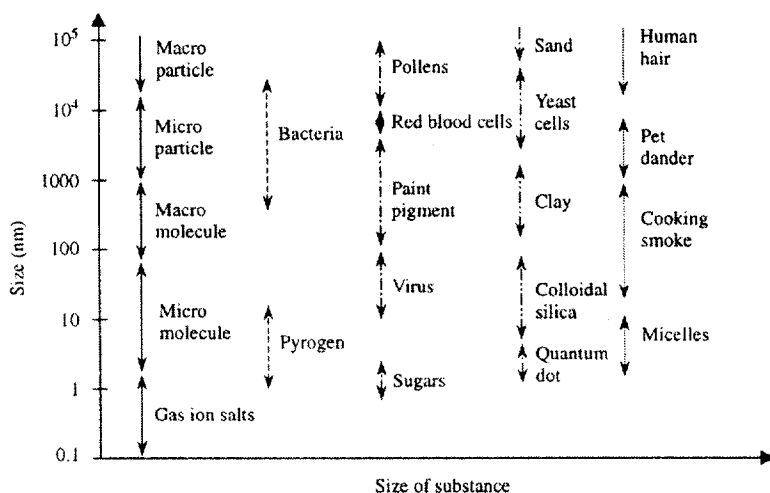


Figure 2-10. Examples of zero-dimensional nanostructures or nanomaterials with their typical ranges of dimension.

Currently there are a lot of different opinions about what exactly is nanotechnology. For example, some people consider the study of microstructures of materials using electron microscopy and the growth and characterization of thin films as nanotechnology. Other people consider a bottom-up approach in materials synthesis and fabrication, such as self-assembly or biomineralization to form hierarchical structures like abalone shell, is nanotechnology. Drug delivery, e.g. by putting drugs inside carbon nanotubes, is considered as nanotechnology. Micro-electromechanical systems (MEMS) and lab-on-a-chip are considered as nanotechnology. More futuristic or

science fiction-like opinions are that nanotechnology means something very ambitious and startlingly new, such as miniature submarines in the bloodstream, smart self-replication nanorobots monitoring our body, space elevators made of nanotubes and the colonization of space. There are many other definitions that people working in nanotechnology use to define the field. These definitions are true to certain specific research fields, but none of them covers the full spectrum of nanotechnology. The many diverse definitions of nanotechnology reflect the fact that nanotechnology covers a broad spectrum of research field and requires true interdisciplinary and multidisciplinary efforts.

In general, nanotechnology can be understood as a technology of design, fabrication and application of nanostructures of physical properties and phenomena of nanomaterials and nanostructures. Study on fundamental relationships between physical properties and phenomena and material dimensions in the nanometer scale, is also referred to as nanoscience.

In order to explore novel physical properties and phenomena and realize potential applications of nanostructures and nanomaterials, the ability of fabricate and process nanomaterials and nanostructures is the first corner stone in nanotechnology. Nanostructured materials are those with at least one dimension falling in nanometer scale, and include nanoparticles (including quantum dots, when exhibiting quantum effect), nanorods and nanowires, thin films, and bulk materials made of nanoscale building blocks or consisting of nanoscale structures. Many technologies have been explored to fabricate nanostructures and nanomaterials. These technical approaches can be grouped in several ways. One way is to group them according to the

growth media.

(1) Vapor phase growth, including laser reaction pyrolysis for nanoparticle synthesis and atomic layer deposition (ALD) for thin film deposition.

(2) Liquid phase growth, including colloidal processing for the formation of nanoparticles and self assembly of monolayers.

(3) Solid phase formation, including phase segregation to make metallic particles in glass matrix and two-photon induced polymerization for the fabrication of three-dimensional photonic crystals.

(4) Hybrid growth, including vapor-liquid-solid (VLS) growth of nanowires.

Another way is to group the techniques according to the form of products:

(1) Nanoparticles by means of colloidal processing, flame combustion and phase segregation.

(2) Nanorods or nanowires by template-based electroplating, solution-liquid-solid growth (SLS), and spontaneous anisotropic growth.

(3) Thin films by molecular beam epitaxy (MBE) and atomic layer deposition (ALD)

(4) Nanostructured bulk materials, for example, photonic bandgap crystals by self-assembly of nanosized particle.

There are many other ways to group different fabrication and processing techniques such as top-down and bottom-up approaches, spontaneous and forced processes. Top-down is in general an extension of lithography. The concept and practice of a bottom-up approach in material science and chemistry are not new either. Synthesis of large polymer molecules is a typical bottom-up approach,

in which individual building blocks (monomers) are assembled to a large molecule or polymerized into bulk material. Crystal growth is another bottom-up approach, where growth species either atoms, or ions or molecules orderly assemble into desired crystal structure on the growth surface.

2-1-2. Basic of ferromagnetism

The value of the magnetic moment of a body is a measure of the strength of the magnetism that is present.^{46,48} Atoms in the various transition series of the periodic table have unfilled inner energy levels in which the spins of the electrons are unpaired, giving the atom a net magnetic moment. The iron atom has 26 electrons circulating about the nucleus. Eighteen of these electrons are in filled energy levels that constitute the argon atom inner core of the electron configuration. The *d* level of the $N=3$ orbit contains only 6 of the possible 10 electrons that would fill it, so it is incomplete to the extent of four electrons. This incompletely filled electron *d* shell causes the iron atom to have a strong magnetic moment.

When crystals such as bulk iron are formed from atoms having a net magnetic moment a number of different situations can occur relating to how the magnetic moments of the individual atoms are aligned with respect to each other. Fig. 2-11 illustrates some of the possible arrangements that can occur in two dimensions. The point of the arrow is the north pole of the tiny bar magnet associated with the atom. If the magnetic moments are randomly arranged with respect to each other, as shown in Fig. 2-11 (a), then the crystal has a zero net magnetic moment, and this is referred to as the *paramagnetic state*. The application of a DC magnetic field aligns some of the

moments all point in the same direction, as shown in Fig. 2-11 (b), even when no DC magnetic field is applied, so the whole crystal has a magnetic moment and behaves like a bar magnet producing a

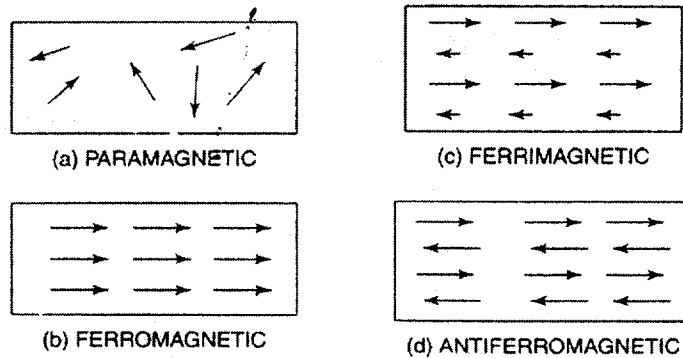


Figure 2-11. Illustration of various arrangements of individual atomic magnetic moments that constitute (a) paramagnetic, (b) ferromagnetic, (c) ferrimagnetic and (d) antiferromagnetic materials.

magnetic field outside of it. If a crystal is made of two types of atoms, each having a magnetic moment of a different strength (indicated in Fig. 2-11 (c) by the length of the arrow) the arrangement shown in Fig. 2-11 (c) can occur, and it is called ferromagnetic. Such a crystal will also have a net magnetic moment, and behave like a bar magnet. In an antiferromagnet the moments are arranged in an antiparallel scheme, that is, opposite to each other, as shown in Fig. 2-11 (d), and hence the material has no net magnetic moment.

2-1-3. Nanostructured magnetic material.

Many of our modern technological devices rely on magnetism and magnetic materials; these include electrical power generators and

transformers, electric motors, computers, and components of sound and video reproduction systems. Novel nanomagnetic materials are interesting from the point of view of the relationship between microstructural features and magnetic properties. Such features include particle size and distribution, chemical inhomogeneities, crystalline defects, crystallographic texture examples being (a) nanocrystalline soft magnetic materials produced from amorphous precursors, (b) two-phase nanoparticles with high moment cores and high resistivity ferrite shells, and (c) spin exchange magnetic materials. Areas of topical interest include soft and hard magnets, hard magnetic nanoparticles, magnetic recording media and magnetic multilayers. Magnetic nanoparticles show a variety of unusual magnetic behaviour compared to bulk materials, mostly due to surface/interface effects, including symmetry breaking, electronic environment/charge transfer, and magnetic interactions. Furthermore, since nanophase particles can be as much as 50% surface material, new magnetic properties characteristic of surfaces and interfaces become important and may be of practical value.

2-1-4. Application of magnetic material

Applications of magnetic materials at DC

Dc was the first type of electrical current discovered so it is natural that the first practical use of magnetic materials was made in DC devices.⁴⁸ The main functions were the conversion of electrical power or the converse. These applications include;

1. DC motors and generators driven by electromagnetic forces created in wound stators and rotors or in permanent magnets.
2. Electro-mechanical devices such as relays, switches, armatures and pole pieces for opening and closing electrical circuits, doorbells, buzzers.

3. Plungers, brakes and transducers for controlling flow, pressure switches

4. Reed switches

Power applications at low frequencies

Low frequency power generation and conditioning are probably the applications that consume the largest tonnage of magnetic materials but not the largest dollar volume. This application mostly involves in the production and distribution of 50 and 60 Hertz line or mains frequencies. The magnetic equipment consists mainly of generators, motors and transformers. As we shall see, cost is the main consideration although in an effort to obtain lower losses, there is a range of properties and costs within the overall product range. For very large generator, there is a compromise between higher operating efficiency and the initial cost of the magnetic material, which is a very large part of the generator cost. For smaller motors and appliances aimed at consumer applications, cost is the determining factor at the expense of efficiency.

Entertainment application

A very large tonnage of magnetic materials goes into the consumer entertainment market. In the radio and television applications, some of the functions for magnetic cores are as follows;

1. Television picture tube yokes
2. Flyback transformers
3. Power transformers
4. Interstage transformers
5. Pin Cushion transformers

6. Radio and television antennae
7. Tuning slugs

Magnetic recording applications

Because of the very large and growing market for all types of magnetic recording and because of the relatively high material cost of the magnetic materials relative to the low frequency power materials for motors and transformers, this application is undoubtedly the highest dollar volume segment. The various components and materials in the broad spectrum of magnetic recording can be classified as follows;

1. Magnetic memory cores
2. Magnetic audio tape
3. Floppy disks
4. Hard disks
5. Video cassette tape
6. Magnetic ink for credit cards
7. Magnetic media
8. Magnetic recording heads
9. Rotary transformers
10. Copier powers
11. Bubble memories
12. Magneto-optic memory disks

2-1-5. Exchange coupled hard/soft magnet

Controlled structuring of materials at the nanoscale can enhance some of their properties and widen their range of application. Magnetic materials, such as recording media, field sensors and memory devices, are advancing

rapidly in terms of their miniaturization, sensitivity and other figures of merit. But progress in producing permanent magnets has been limited by the difficulty of finding new compounds with the necessary properties.

The figure of merit by which permanent-magnet materials are judged is the energy product a measure of the maximum magnetostatic energy that would be stored in free space between the pole pieces of a magnet made from the material in question.⁴⁹ The energy product depends on the area of the 'hysteresis loop'. A typical hysteresis loop arises from plotting the magnetization of the material as the applied magnetic field is varied the response of the materials follows two distinct paths on magnetization and demagnetization. As well as the saturation point (maximum magnetization), the hysteresis loop is characterized by the 'coercivity' of the material, which is the reverse-field strength needed to reduce the flux density to zero. To obtain a large energy product requires large magnetization and large coercivity.

The largest energy product observed in nature, for the compound $\text{Nd}_2\text{Fe}_{14}\text{B}$, is 56.7 MGOe. $\text{Nd}_2\text{Fe}_{14}\text{B}$ has a complex structure containing 68 atoms in its unit cell. The Nd-Fe-B class of magnets owes its position as the highest-energy magnet to its high magnetization (mainly from Fe ions) and to its tetragonal structure and Nd ions, which together produce a high degree of magnetic anisotropy. This anisotropy in turn causes high coercivity.

About a decade ago, an idea emerged that brought new hope. This is the concept of 'exchange coupling' between a hard (high-coercivity) material and a soft (low-coercivity) material with a large magnetization. In a two-phase mixture of such materials, exchange forces between the phases mean the resulting magnetization and coercivity of the material will be some average of the properties of the two constituent phases.⁵⁰ But for the exchange coupling to be effective, the relative sizes of the grains of the two

materials must be chosen carefully: Kneller and Hawig⁵¹ showed that the characteristic dimensions of the soft phase cannot exceed about twice the wall thickness of magnetic domains in the hard phase. Typically, this limits the soft phase to grains of about 10 nm diameter. Similarly, the hard phase must have dimensions of this order or the volume fraction of the soft phase will be rather low, thus limiting the magnetization of the composite.

Skomski and Coey⁵⁰ showed that in an ideal exchange-coupled magnet, consisting of aligned grains of $\text{Sm}_2\text{Fe}_{17}\text{N}_3$ and $\text{Fe}_{65}\text{Co}_{35}$, the theoretical upper bound on the energy product is about 125 MGOe. But in the real world, attempts to fabricate two-phase nanostructures with a high energy product have had only limited success. Bulk magnets produced by subjecting the two-phase material to ultra-fast cooling and then annealing, or by mechanical milling, have not achieved energy products beyond about 20 MGOe.⁵² There are several difficulties to be overcome: controlling the material structure at the nanoscale, especially to create uniform grain sizes of about 10 nm; aligning the hard grains sufficiently; and ensuring effective exchange coupling between the two phases in all grains through an homogeneous distribution.

2-1-6. Synthetic method of nanosized-magnetic materials

2-1-6-1. Polyol process

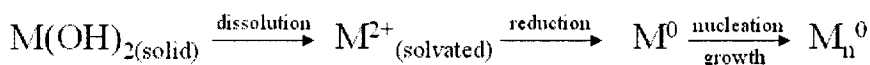
Over the past few years, this process has been developed to prepare finely divided powders of various metals: cobalt, nickel, lead, silver, copper, palladium and some of these metals' alloys. The general method of synthesis is the following: an inorganic metallic compound or salt is dispersed in a liquid polyol. Ethylene glycol is mainly used. The suspension is then stirred and heated to a given temperature, until complete reduction of the

compound. The metal is then recovered as a finely divided powder by centrifugation or filtration^{3, 53}. The obtained particles are monodisperse, non-agglomerated, in the colloidal or micronic range⁵⁴⁻⁵⁷. In the particular case of the polyol process, a metallic powder is said to be monodisperse when the variation coefficient of the particle size distribution does not exceed 20%. As a matter of fact, the instrumental error during the particle size distribution measurement has to be taken into account, as well as the fact that it is impossible to obtain a perfect system of monosized and monoshaped particles.

Monodisperse particles have been obtained from precursors such as acetate, hydroxide or hydroxycarbonate in ethylene glycol or mixture of ethylene glycol and diethylene glycol^{3,58}. The reaction is not a solid phase transformation but proceeds according to the following scheme:

- progressive dissolution of the solid precursor;
- reduction of the dissolved species by the polyol itself;
- nucleation and growth of the metal particles from the solution.

Therefore polyol acts simultaneously as the dispersing medium, the solvent, the reducing agent and the crystal growth medium for the metal particles. The dissolution of this solid phase which acts as a reservoir for the Mⁿ solvated species, controls the concentration of these species according to Scheme 1.⁵⁹

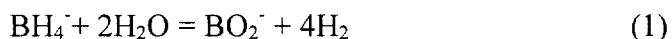


Scheme 1. Mechanism of precipitation of metal particles from corresponding hydroxide.

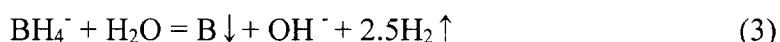
2-1-6-2. Co-precipitation route

Mechanism of the reactions. The hydrolysis reaction of borohydride for the

generation of H₂ was established ⁶⁰:

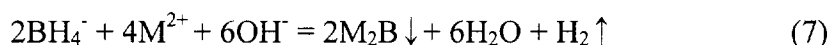
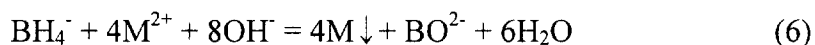
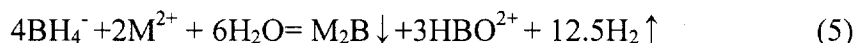
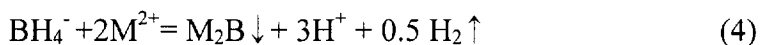


which can be greatly accelerated by H⁺ or metals such as Fe, Co, and Ni. Thus, this hydrolysis reaction may accompany reactions between borohydride and metal ions in aqueous solutions for the production of M-B (M = Fe, Co, Ni, etc.) ultrafine amorphous alloy particles (UFAAP). Assuming that the reductions of metal ions and B³⁺ are independent each other, the formation processes of metals and boron in the products can be expressed as below according to the mass and charge balances:



Equation 3 is actually a combination of the half-reactions (h) and (d'). In the literature, different overall reactions for producing Co-B and Ni-B have been suggested.⁶¹ Here, we list the same equations representing the possible overall reactions for producing

M-B UFAAP:



2-2. Materials and Method

2-2-1. Preparation Co nanoparticle by polyol method

2-2-1-1. Preparation of Co nanoparticle by polyol method

The cobalt chloride hexahydrate ($\text{CoCl}_2 \cdot 6\text{H}_2\text{O}$, 98%+), sodium hydroxide (NaOH , 97%+) and ethylene glycol ($\text{HOCH}_2\text{CH}_2\text{OH}$, 99%+) were purchased from Aldrich Chemical Co. and used without purification. The preparation for Co nanoparticles was carried out under nitrogen. To prepare the Co particles, 10 mmol of $\text{CoCl}_2 \cdot 6\text{H}_2\text{O}$ and 50 mmol of NaOH were mixed in 100 ml deoxygenated ethylene glycol (100 ml, nitrogen gas bubbling for 30 min) then heated to 110 °C. The mixture was refluxed for 3 hrs at the 220 °C. After it was cooled to room temperature, the precipitate was separated and washed with deoxygenated water (100 ml, nitrogen gas bubbling for 30 min) to remove residue Cl^- and Na^+ ions, then washed with acetone and dried with nitrogen gas. The product was stored in cyclohexane.

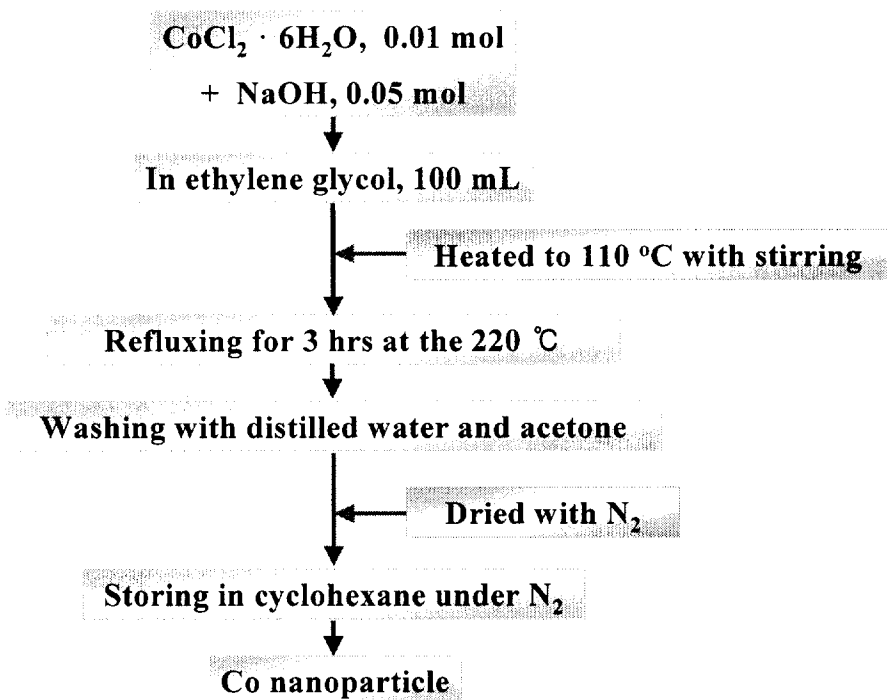


Figure 2-1. The preparation process of Co nanoparticles by polyol method.

2-2-1-2. Preparation of Co nanoparticle according to different precursors and size control

Cobalt acetate tetrahydrate ($\text{Co}(\text{CH}_3\text{CO}_2)_4 \cdot 4\text{H}_2\text{O}$, 95%), cobalt hydroxide, ($\text{Co}(\text{OH})_2$, 95%), sodium hydroxide (NaOH, 97%+), 1,2-propanediol (99%) and oleic acid ($\text{CH}_3(\text{CH}_2)_7\text{CH}=\text{CH}(\text{CH}_2)_7\text{COOH}$, 99%+) were purchased from Aldrich Chemical Co. and used without purification. The preparation for Co nanoparticles was carried out under nitrogen. To prepare Co nanoparticles, 10 mmol of $\text{Co}(\text{CH}_3\text{CO}_2)_2 \cdot 4\text{H}_2\text{O}$ or $\text{Co}(\text{OH})_2$ and 50 mmol of NaOH were mixed in 100 ml deoxygenated 1,2-propanediol (100 ml, nitrogen gas bubbling for 30 min) then heated to 110 °C. Oleic acid (1 mmol) was injected into the mixture. The mixture was refluxed for 3 hrs at

220 °C. After cooled to room temperature, the precipitate was separated and washed with deoxygenated water (100 ml, nitrogen gas bubbling for 30 min) to remove residue Cl^- and Na^+ ions, then washed with acetone and dried with nitrogen gas. The product was stored in cyclohexane.

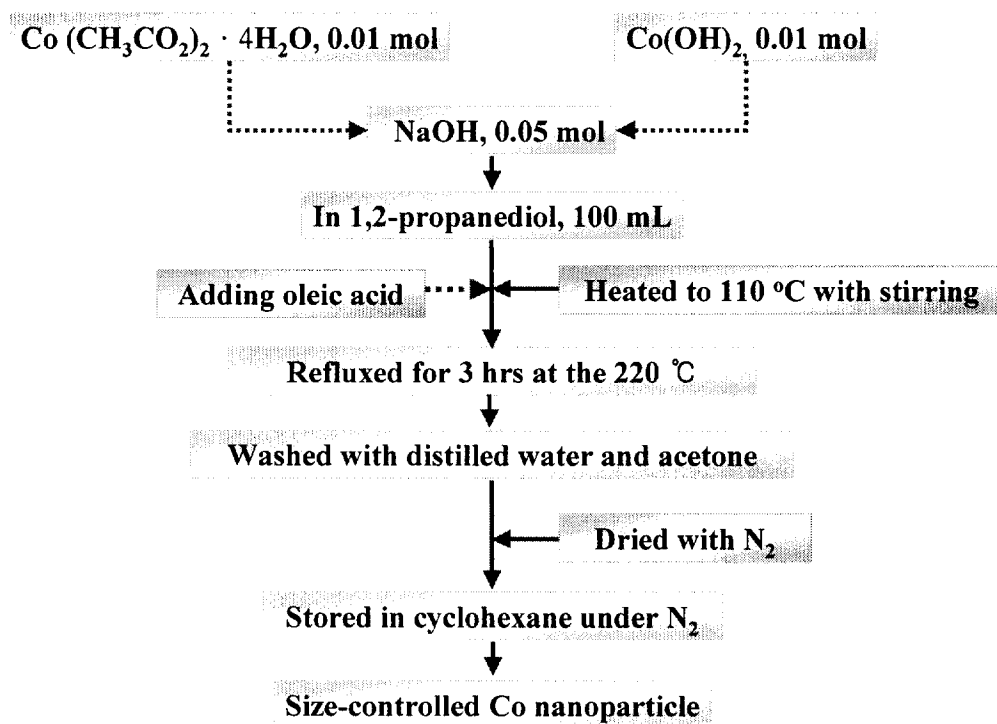


Figure 2-2. The preparation process of Co nanoparticles by size control.

2-2-2. Preparation of Co nanoparticle by new solventless thermal decomposition

The preparation for the Co nanoparticles was carried out under nitrogen. Cobalt chloride hexahydrate ($\text{CoCl}_2 \cdot 6\text{H}_2\text{O}$, 98%+), sodium oleate ($\text{CH}_3(\text{CH}_2)_7\text{CH}=\text{CH}(\text{CH})_7\text{COONa}$, 98%+) and cyclohexane (C_6H_{12} , 99.5%+) were purchased from Aldrich Chemical Co. and used without further

purification. Cobalt chloride hexahydrate was used as the initial material. The distilled water was purged with nitrogen gas for 1 hr before reaction. To prepare the Co^{2+} -oleate₂ complex, 1.4276 g of $\text{CoCl}_2 \cdot 6\text{H}_2\text{O}$ (6 mmol) was dissolved in deoxygenated water (50 ml, nitrogen gas bubbling for 30 min) and 3.6534 g of sodium oleate (12 mmol) was dissolved in deoxygenated water (150 ml, nitrogen gas bubbling for 30 min). The metal solution was added into the sodium oleate solution drop by drop under vigorous stirring for 30 min. The precipitate was separated by filtration and washed with distilled water to remove sodium and chloride ions. After drying it completely, Co^{2+} -oleate₂ complex was put into the pyrex tube. The complex in the pyrex tube was flushed with nitrogen gas first, and then the tube was sealed at low pressure (0.8 torr). The sample was slowly heated up to 400 °C by 1 °C/min. After reaching the desired temperature, it was held at 400 °C for 3 hrs and cooled to room temperature. The complex color was changed to black. The black product was washed with chloroform to separate oleate and distilled water to remove residue ions, then washed with acetone. The product was dried with nitrogen gas and stored in cyclohexane.

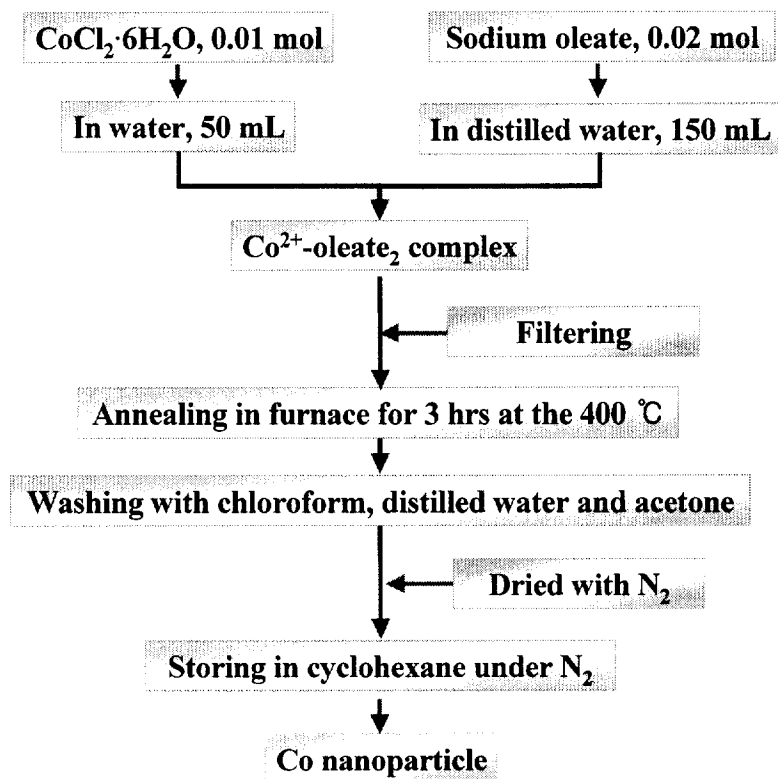


Figure 2-3. The preparation process of Co nanoparticles by solventless thermal decomposition.

2-2-3. Preparation of Co nanoparticle by co-precipitation route

The preparation for Co the nanoparticles was carried out under nitrogen. $\text{CoCl}_2 \cdot 6\text{H}_2\text{O}$ (98%+) and NaBH_4 (98%) were purchased from Aldrich Chemical Co. and used without further purification. 10 mmol of $\text{CoCl}_2 \cdot 6\text{H}_2\text{O}$ were dissolved in deoxygenated water (100 ml, nitrogen gas bubbling for 30 min). 10 mmol of NaBH_4 was dissolved in 50 ml deoxygenated water. NaBH_4 solution was dropped into metal solution by using dropping funnel with stirring under nitrogen atmosphere. The black precipitate was obtained together with formation of hydrogen gas. After the precipitate was

formed, it was washed with distilled water to remove impurities and washed with acetone, then dried with nitrogen gas. The product was stored in cyclohexane.

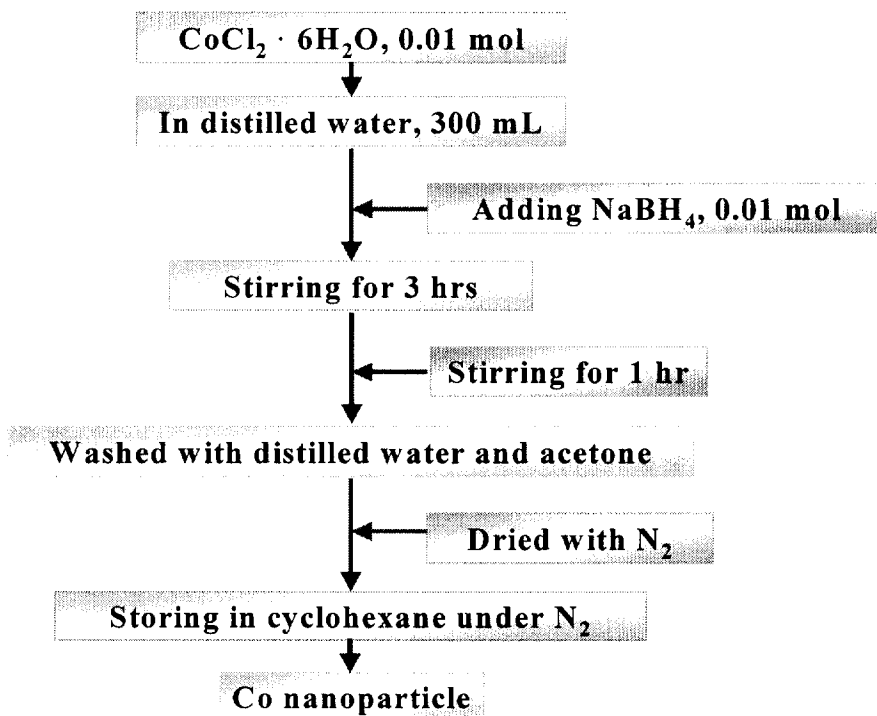


Figure 2-4. The preparation process of Co nanoparticles by co-precipitation route.

2-1-4. Preparation of FeCo nanoparticle by polyol method

2-2-4-1. Preparation of FeCo nanoparticle by polyol process

The preparation for the FeCo nanoparticles was carried out under nitrogen gas. Fe(CH₃CO₂)₂·4H₂O(95%+), Co(CH₃CO₂)₂·4H₂O (98%+), oleic acid (CH₃(CH₂)₇CH=CH(CH₂)₇COOH, 99%+) and 1,2-propanediol (99%) were purchased from Aldrich Chemical Co. and used without further purification.

To prepare FeCo nanoparticle, 1 mmol $\text{Fe}(\text{CH}_3\text{CO}_2)_2 \cdot 4\text{H}_2\text{O}$, 5 mmol of $\text{Co}(\text{CH}_3\text{CO}_2)_2 \cdot 6\text{H}_2\text{O}$ and 30 mmol of sodium hydroxide were mixed in deoxygenated 1,2-propanediol (60 ml, nitrogen gas bubbling for 30 min). The mixture was heated to 110 °C. Oleic acid was injected to reactant, then refluxed for 3 hrs at the 220 °C. After cooled to room temperature, the precipitate was separated and washed with distilled water and acetone then dried with nitrogen gas. The product was stored in cyclohexane.

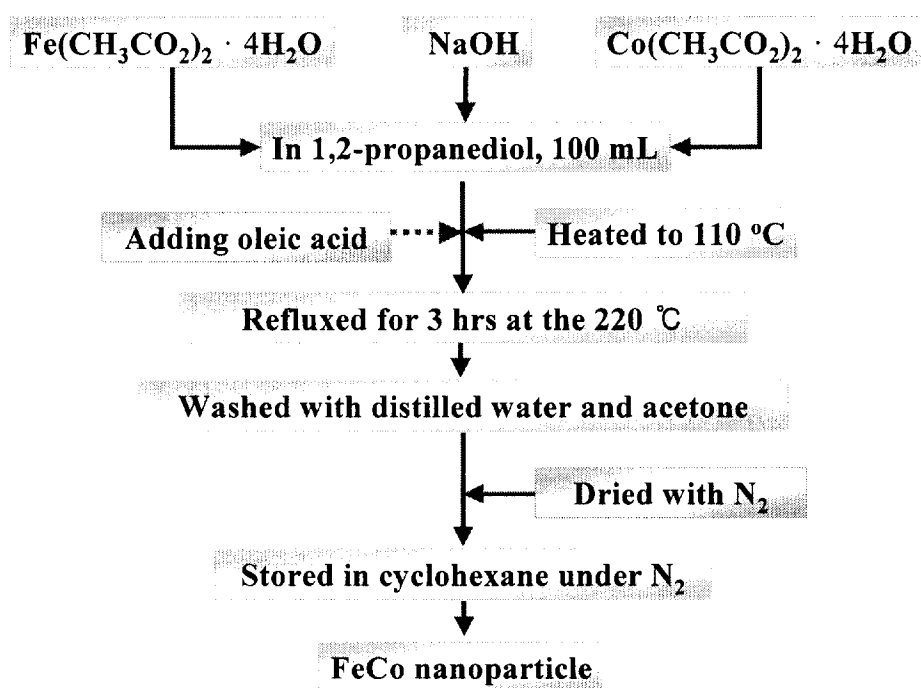


Figure 2-5. The preparation process of FeCo nanoparticles by polyol method.

2-2-5. Preparation of FeCo nanoparticle by co-precipitation route

2-2-5-1. Preparation of FeCo nanoparticle by coprecipitation route

The preparation for the FeCo nanoparticles was carried out under nitrogen gas. $\text{FeCl}_2 \cdot 4\text{H}_2\text{O}$ (99%+), $\text{CoCl}_2 \cdot 6\text{H}_2\text{O}$ (98%+) and NaBH_4 (98%) were purchased from Aldrich Chemical Co. and used without further purification. 7 mmol of $\text{FeCl}_2 \cdot 4\text{H}_2\text{O}$ and 3 mmol of $\text{CoCl}_2 \cdot 6\text{H}_2\text{O}$ were dissolved in deoxygenated water (200 ml, nitrogen gas bubbling for 30 min). 10 mmol of NaBH_4 was dissolved in 50 ml deoxygenated water. NaBH_4 solution was dropped into the metal solution by using dropping funnel with stirring under nitrogen atmosphere. The black precipitate was obtained together with formation of hydrogen gas. After precipitate was formed, it was washed with distilled water to remove residue Na^+ and Cl^- ions and washed acetone then dried with nitrogen gas. The product was stored in cyclohexane.

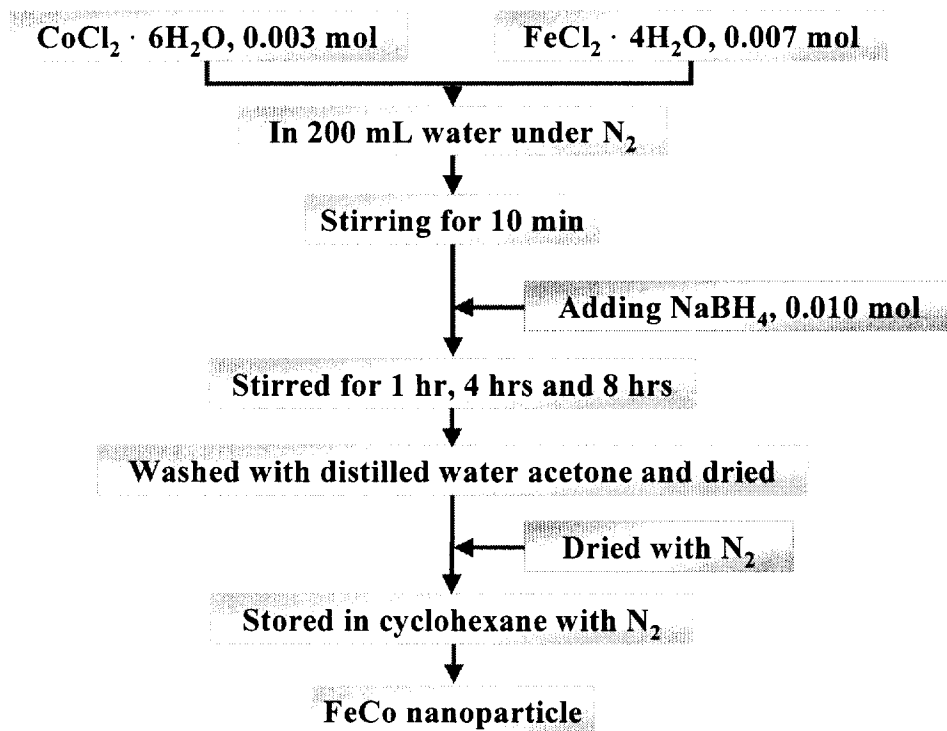


Figure 2-6. The preparation process of FeCo nanoparticles by co-precipitation route.

2-2-5-2. Preparation of FeCo nanoparticle according to different precursors

The preparation for the FeCo nanoparticles was carried out under nitrogen. $\text{Fe}(\text{CH}_3\text{CO}_2)_2 \cdot 4\text{H}_2\text{O}$ (95%), $\text{Co}(\text{CH}_3\text{CO}_2)_2 \cdot 4\text{H}_2\text{O}$ (98%+) or $\text{Co}(\text{OH})_2$ (95%) and NaBH_4 (98%) were purchased from Aldrich Chemical Co. and used without further purification. 7 mmol of $\text{Fe}(\text{CH}_3\text{CO}_2)_2 \cdot 4\text{H}_2\text{O}$ (95%) and 3 mmol of $\text{Co}(\text{CH}_3\text{CO}_2)_2 \cdot 4\text{H}_2\text{O}$ (98%+) or $\text{Co}(\text{OH})_2$ (95%) were dissolved in deoxygenated water (200 ml, nitrogen gas bubbling for 30 min). 10 mmol of NaBH_4 was dissolved in 50 ml deoxygenated water. NaBH_4 solution was dropped into the metal solution by using dropping funnel with stirring under

nitrogen atmosphere. The black precipitate was obtained together with formation of hydrogen gas. After precipitate was formed, it was washed with distilled water to remove impurities and washed acetone then dried with nitrogen gas. The product was stored in cyclohexane.

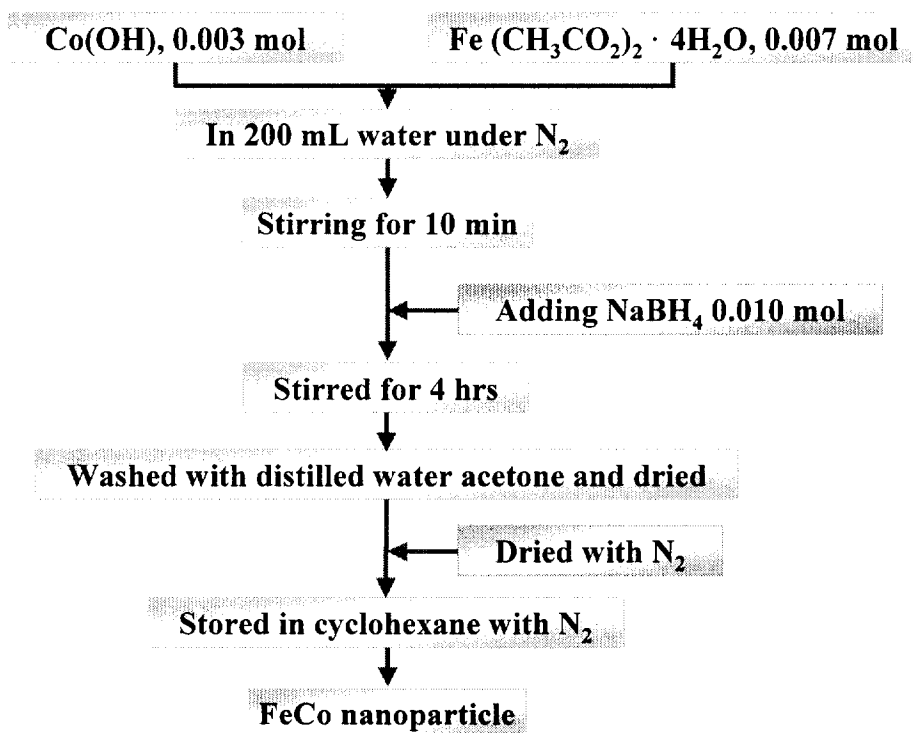


Figure 2-7. The preparation process of FeCo nanoparticles by co-precipitation route according to different precursors.

2-2-6. Preparation of CoFe_2O_4 nanoparticle by polyol method

The preparation for the CoFe_2O_4 nanoparticles was carried out under nitrogen. $\text{FeCl}_2 \cdot 4\text{H}_2\text{O}$ (95%+), $\text{CoCl}_2 \cdot 6\text{H}_2\text{O}$ (98%+) and 1,2-propanediol (99%) were purchased from Aldrich Chemical Co. and used without further purification. To prepare the CoFe_2O_4 nanoparticle, 3.3 mmol $\text{FeCl}_2 \cdot 4\text{H}_2\text{O}$, 6.6 mmol of $\text{CoCl}_2 \cdot 6\text{H}_2\text{O}$ and 60 mmol of sodium hydroxide were mixed in

deoxygenated 1,2-propanediol (100 ml, nitrogen gas bubbling for 30 min). The mixture was heated to 110 °C then refluxed for 3 hrs at the 220 °C. After cooled to room temperature, the precipitate was separated and washed with distilled water and acetone then dried. The product was stored in cyclohexane.

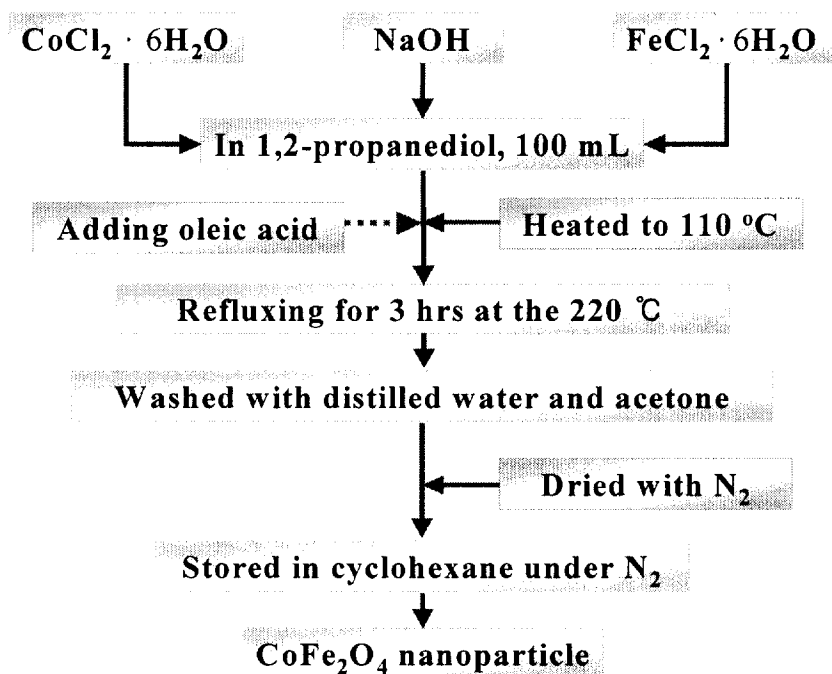


Figure 2-8. The preparation process of CoFe₂O₄ nanoparticles by polyol method.

2-2-7. Preparation of SmCo nanoparticle by new solvetless thermal decomposition

The preparation for the SmCo nanoparticles was carried out under argon. Samarium chloride hexahydrate (SmCl₂·6H₂O, 99.99%+), cobalt chloride hexahydrate (CoCl₂·6H₂O, 98%+), cyclohexane (C₆H₁₂, 99.5%+) and sodium oleate (CH₃(CH₂)₇CH=CH(CH₂)₇COONa, 98%+) were purchased from

Aldrich Chemical Co. and used without further purification. Samarium chloride hexahydrate and cobalt chloride hexahydrate were used as initial material. The distilled water was purged with argon gas for 1 hr before reaction. To prepare the mixture of the Sm^{2+} -oleate₂ and Co^{2+} -oleate₂ complexes, 0.3648 g of $\text{SmCl}_3 \cdot 6\text{H}_2\text{O}$ (1 mmol) and 1.1897 g of $\text{CoCl}_2 \cdot 6\text{H}_2\text{O}$ (5 mmol) were dissolved in deoxygenated water (50 ml, argon gas bubbling for 30 min) and 3.9578 g of sodium oleate (13 mmol) was dissolved in deoxygenated water (150 ml, argon gas bubbling for 30 min). The metal solution was added into a sodium oleate solution drop by drop under vigorous stirring for 30 min. The precipitate was separated by filtration and washed with distilled water to remove sodium and chloride ions. After drying perfectly, the mixture of the Sm^{2+} -oleate₂ and Co^{2+} -oleate₂ complexes was put into the pyrex tube. The complexes in the pyrex tube were flushed with argon gas first, and then the tube was sealed at low pressure (0.8 torr). The sample was slowly heated up to 400 °C by 1 °C/min. After reaching the desired temperature, it was held at 400 °C for 3 hrs and cooled to room temperature. The color of the complexes was changed to black. The black product was washed with chloroform to separate oleate and distilled water to remove residue ions, then washed with acetone. The product was dried with argon gas and stored in cyclohexane.

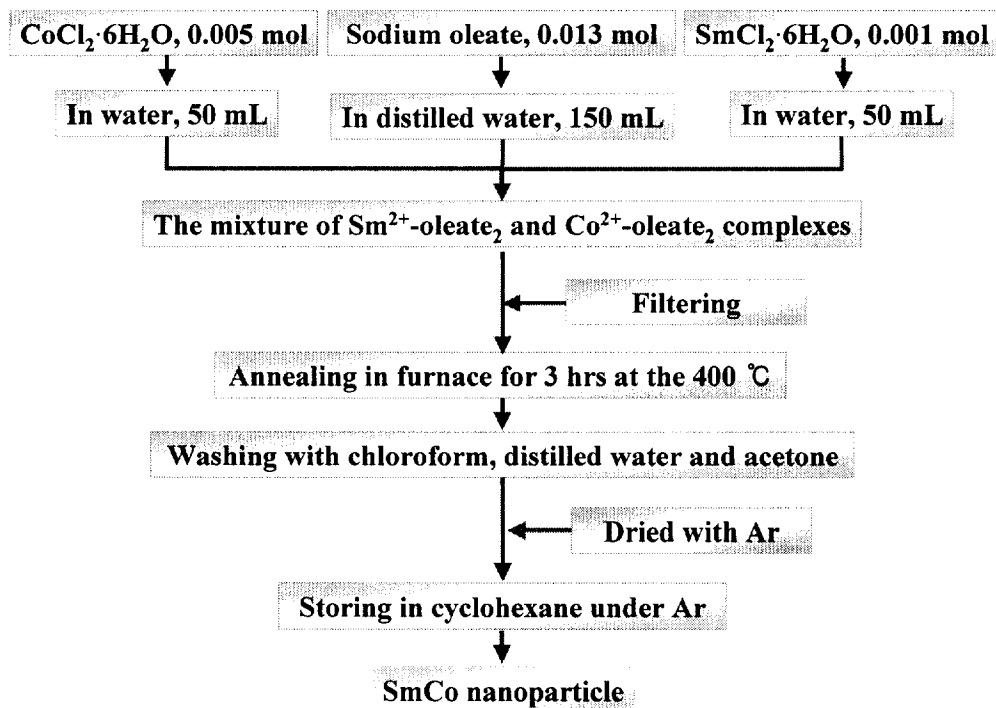


Figure 2-9. The preparation process of SmCo nanoparticles by new solventless thermal decomposition.

2-2-8. Preparation of $\text{Nd}_2\text{Fe}_{14}\text{B}$ alloy by ball milling

$\text{Nd}_{15}\text{Fe}_{77}\text{B}_8$ ingot was smashed into fine pieces by a hammer. The surface of fragment was rubbed by a grinder to remove a oxidated layer. The sample was wrapped with Al_2O_3 tube (10^{-6} mbar) then was homogenized at 1070 °C for 72 hrs. After the homogenization treatment, the oxidated layer was rubbed again. The sample was sealed in glove box under argon, then pulverized by shake milling for 20 hrs. The powder was stored in cyclohexane.

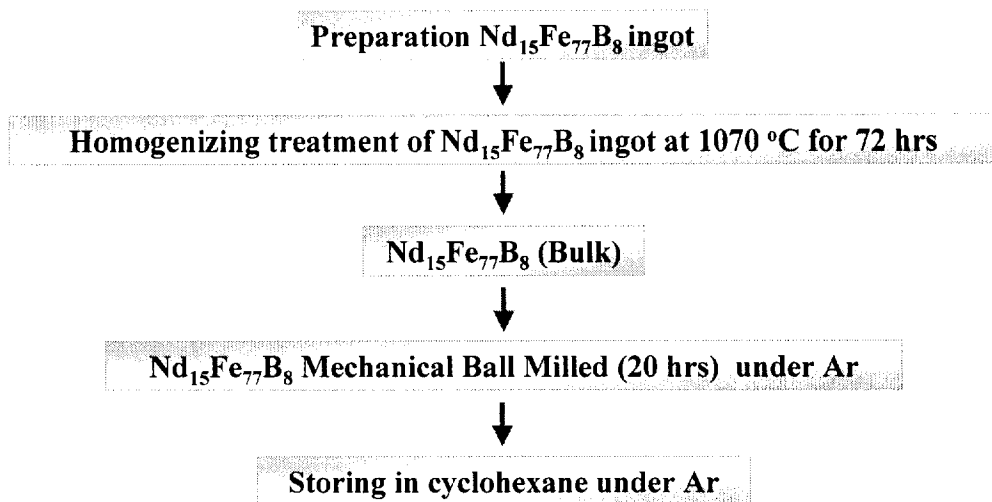


Figure 2-10. The preparation process of $\text{Nd}_2\text{Fe}_{14}\text{B}$ powder by ball milling.

2-2-8. Preparation of $\text{Nd}_2\text{Fe}_{14}\text{B}/\text{Co}$ nanocomposites by colloidal process

The preparation for the $\text{Nd}_2\text{Fe}_{14}\text{B}/\text{Co}$ nanocomposites was carried out under argon. $\text{Co}(\text{CH}_3\text{CO}_2)_2 \cdot 4\text{H}_2\text{O}$ (98%+) and NaBH_4 (98%) were purchased from Aldrich Chemical Co. and used without further purification. 0.5 mmol of $\text{Co}(\text{CH}_3\text{CO}_2)_2 \cdot 4\text{H}_2\text{O}$ were dissolved in deoxygenated water (100 ml, argon gas bubbling for 30 min). 0.5 mmol of NaBH_4 was dissolved in 50 ml deoxygenated water. The amorphous $\text{Nd}_2\text{Fe}_{14}\text{B}$ was put into metal solution. NaBH_4 solution was dropped into the metal solution by using dropping funnel with stirring under argon atmosphere. The black precipitate was obtained together with formation of hydrogen gas. After precipitate was formed, it was washed with distilled water to remove impurities and washed acetone then dried with nitrogen gas. The product was stored in cyclohexane. The sample was annealed at 650 °C for 1 hr in vacuum.

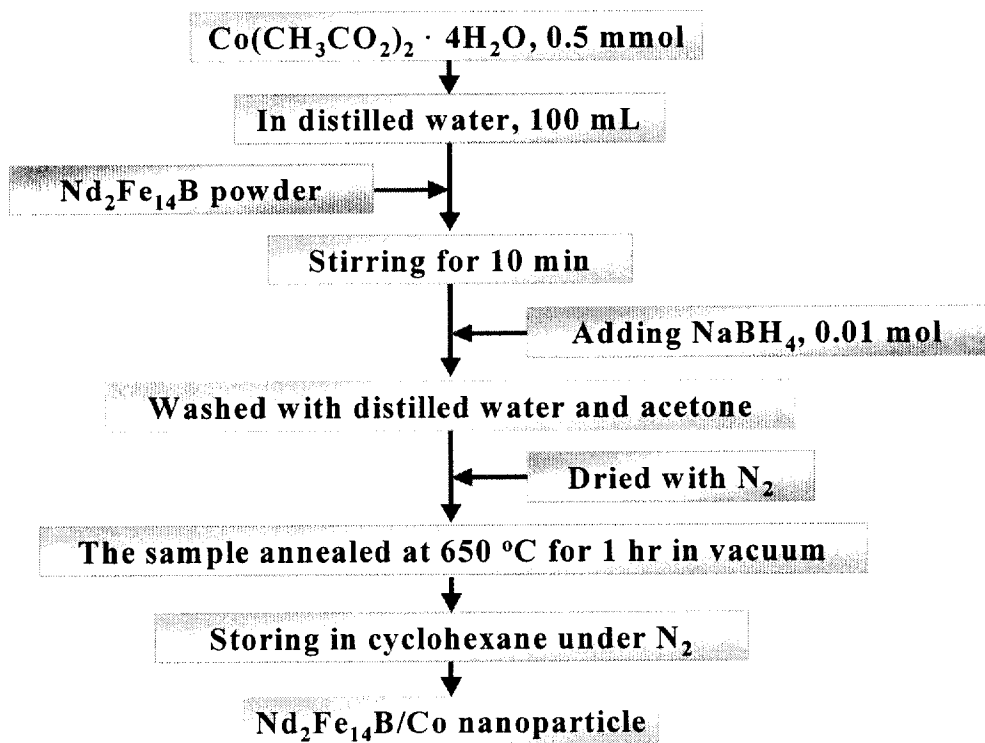


Figure 2-11. The preparation process of Nd₂Fe₁₄B/Co core-shell type nanocomposite.

2-3. Apparatus

Structural characterization of the products was done with transmission electron microscopes (TEM, HITACHI H-7500) and high resolution TEM (JEOL JEM 2010) and X-ray powder diffraction (XRD, Philips X'pert-MPD system). The nanoparticles were characterized by scanning electron microscope energy dispersive X-ray spectrometer (SEM-DES, Hitachi S-2400) and electron probe X-ray micro analyzer (EPMA, shimazu EPMA-1600). The decomposition of the mixture of the Sm²⁺-oleate₂ and Co²⁺-oleate₂ complexes was analyzed with thermogravimetric analysis (TGA, Perkin-elmer TGA 7). The

morphology of the particle was characterized by field emission scanning electron microscope (FE-SEM, JSM-6700F). The magnetic properties were confirmed by superconducting quantum interference device (SQUID, Quantum Design, MPMS XL 7) and vibrating sample magnetometer (VSM, Lake Shore 7300).

3. Results and Discussion

3-1. Preparation of Co nanoparticle

3-1-1. Characterization of Co nanoparticle prepared by polyol method

3-1-1-1. XRD

Fig. 3-1 shows the XRD patterns of the Co nanoparticles. The crystal structures of the Co nanoparticle have been confirmed as fcc and hcp phase. The micron size of the Co nanoparticle that has hcp phase was prepared with cobalt acetate in ethylene glycol. The XRD patterns of the Co nanoparticle samples are shown in Fig. 3-1. The peaks in Fig. 3-1 (a) can be indexed to (100), (002), (101), (110) and (103) planes of a hexagonal unit cell, which corresponds to that of cobalt structure (JCPDS card no. 05-0727). The nano sized-Co particle that has fcc phase was prepared with cobalt acetate (Fig. 3-1 (b)) and cobalt hydroxide (Fig. 3-1 (c)) in 1,2-propanediol. The XRD pattern of Fig. 1 (b) has three main peaks at $2\theta = 44.169, 51.265$ and 76.282 , corresponding to the (110), (200) and (220) plane of a cubic unit cell (JCPDS card, no.15-0806). No other cobalt oxide peak in XRD patterns was detected. It is shown as the difference of crystalline structures of two Co nanoparticle according to different precursors. Fig. 3-2 shows XRD pattern of Co nanoparticle annealed at 800°C for 1 hr. After heat treatment, it shows the high crystallinity. The discernible peaks in Fig. 3-2 can be indexed to (111), (200) and (220) planes of cubic unit cell.

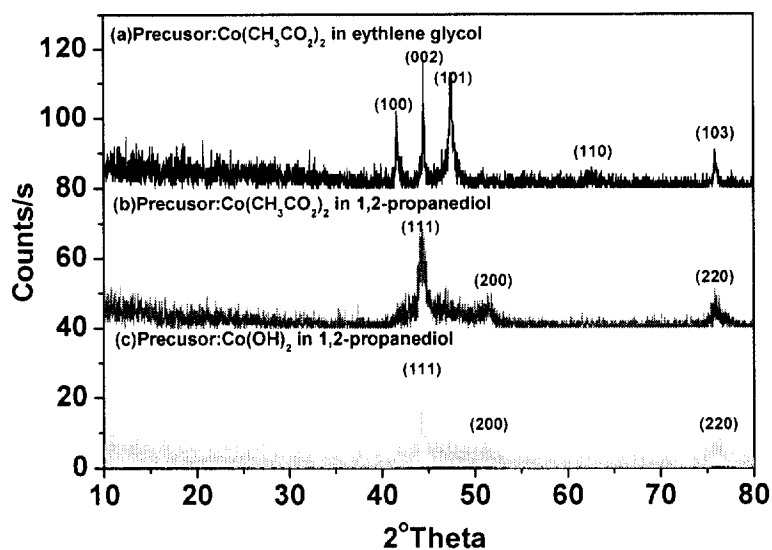


Figure 3-1. XRD patterns of Co nanoparticle according to different precursors.

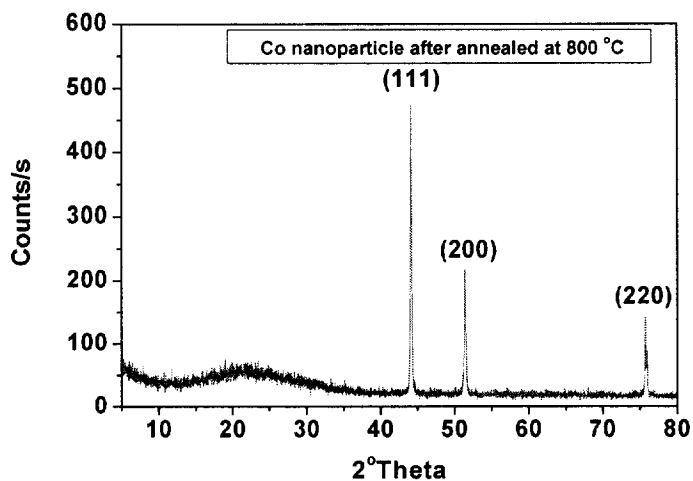


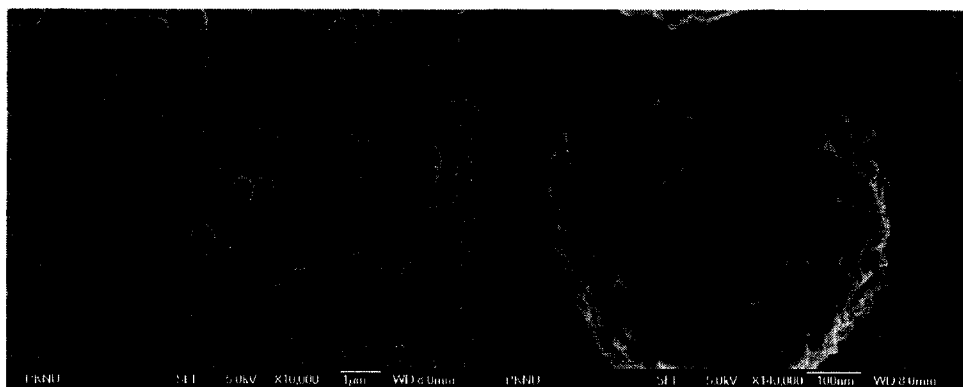
Figure 3-2. XRD patterns of Co nanoparticle after annealed at 800 °C.

3-1-1-2. FE-SEM images

The morphology of the Co nanoparticles was characterized by SEM images (Fig. 3-3). The grain size for nanoparticles was controlled according to different solvents that have different reduction abilities. When ethylene glycol was used as solvent, the grain size was about 800 nm (Fig. 3-3 (a)) . On the other hand, when 1,2-propanediol is used, the reduced size was confirmed and the particle size was uniformly distributed (Fig. 3-3 (b)-(e)). Generally, to control of the size of particles, surfactants were added to reactants. However, this organic compound causes remarkable decrease of magnetic properties. When the metal ion is nucleated in high boiling point of ethylene glycol, the metal particles are surrounded with lone pair electron of oxygen of 2,3-butanedione as surfactant does. When 1,2-propanediol is used instead of ethylene glycol as solvent, 3,4-hexanedione is formed. It causes that space between particles is expanded. Then the particle size is regulated and controlled without surfactant such as oleic acid, triphenylphosphine (TPP)⁶² and polyvinylpyrrolidone (PVP).⁶³

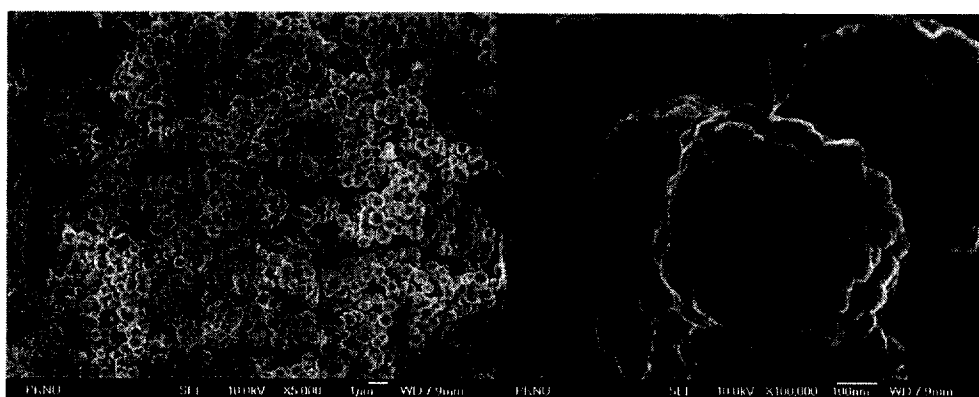


(a)



(b)

(c)



(d)

(e)

Figure 3-3. FE-SEM images of Co nanoparticles according to different precursors. : (a) Co particle (precursor : $\text{Co}(\text{CH}_3\text{CO}_2)_2$ in ethylene glycol) (x50,000), (b) Co nanoparticle (precursor : $\text{Co}(\text{CH}_3\text{CO}_2)_2$ in 1,2-propanediol) (x10,000), (c) Co nanoparticle (precursor : $\text{Co}(\text{CH}_3\text{CO}_2)_2$ in 1,2-propanediol) (x140,000), (d) Co nanoparticle (precursor : $\text{Co}(\text{OH})_2$ in 1,2-propanediol) (x5,000) and (e) Co nanoparticle (precursor : $\text{Co}(\text{OH})_2$ in 1,2-propanediol) (x100,000).

3-1-1-3. TEM images

TEM micrographs of the Co nanoparticles prepared in 1,2-propanediol are shown in Fig. 3-4. TEM samples were formed when a drop of the nanoparticle in iso-octane solution was carefully placed on the grid and dried in air. In Fig. 3-4 (a), the diameter of the Co nanoparticle prepared with cobalt acetate was about 40 nm. Fig. 3-4 (b) and (c) images show the Co nanoparticles prepared in 1,2-propanediol. When the particle was not dispersed under the sonication, overall particles are aggregated (Fig. 3-4 (b)). After sonication for 1 hr, Co nanoparticles have definitional images and uniform size (Fig. 3-4 (c)). And Fig. 3-5 shows TEM lattice image for one particle indicating highly crystalline structure. Co lattice spacing of 2.05 Å was consistent with the lattice spacing of (111) plane of Co crystal structure. That means that Co nanoparticle is formed as single domain.



(a)

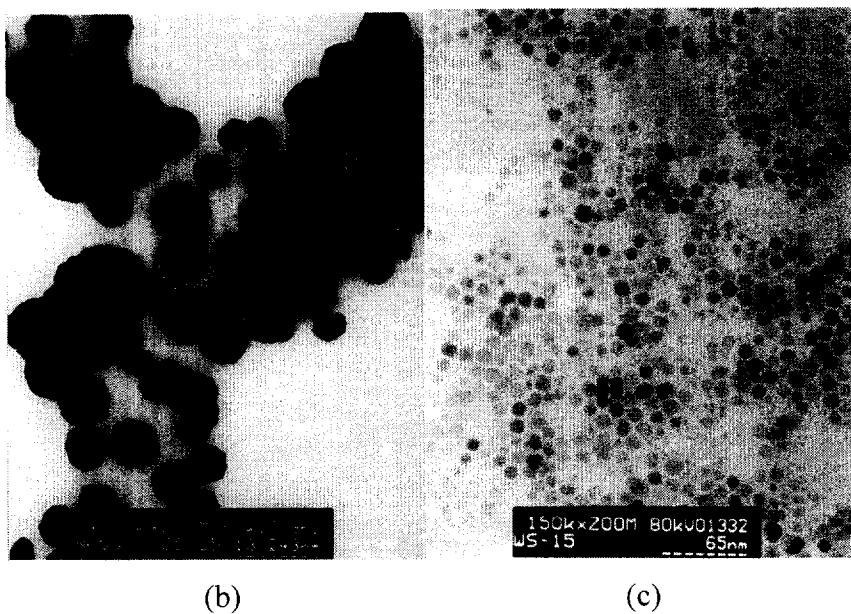


Figure 3-4. TEM images of Co nanoparticles
 (a) Co nanoparticle (precursor : $\text{Co}(\text{CH}_3\text{CO}_2)_2$ in 1,2-propanediol),
 (b) Co nanoparticle (precursor : $\text{Co}(\text{OH})_2$ in 1,2-propanediol)
 before sonication and (c) Co nanoparticle (precursor : $\text{Co}(\text{OH})_2$ in
 1,2-propanediol) after sonication.

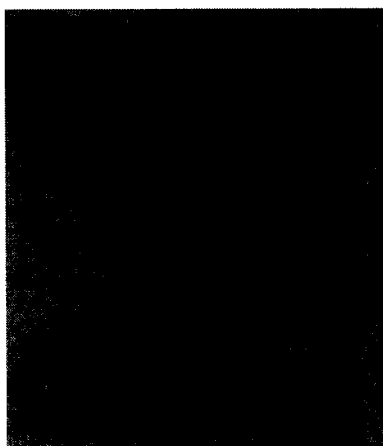


Figure 3-5. HR-TEM image of Co nanocrystallite single domain.

3-1-1-4. SEM-EDX

SEM-EDS analysis (Fig. 3-6) was carried out for the Co nanoparticles by an electron beam (200 kV) to obtain contents of sample. Fig. 3-6 indicates in order the content Co is 100%. Co particle was not oxidized. Besides, there is no impurity except cobalt component. Washing the product sufficiently is absolutely necessary to obtain pure product not including contents of Na^+ and Cl^- ions.

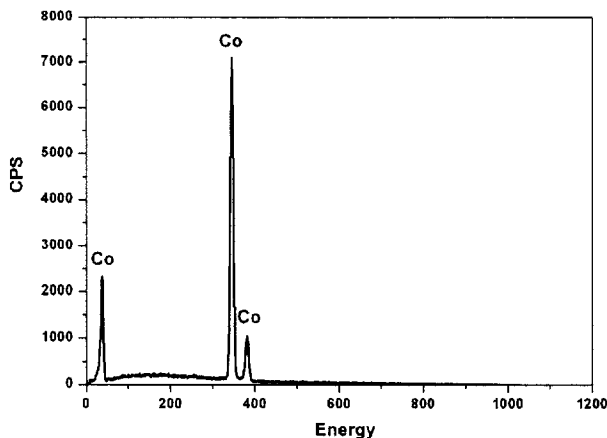
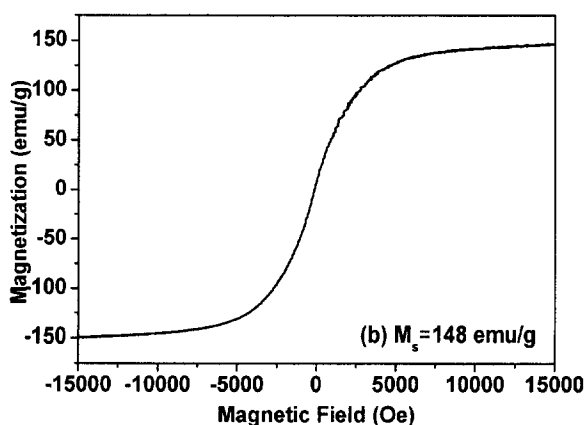
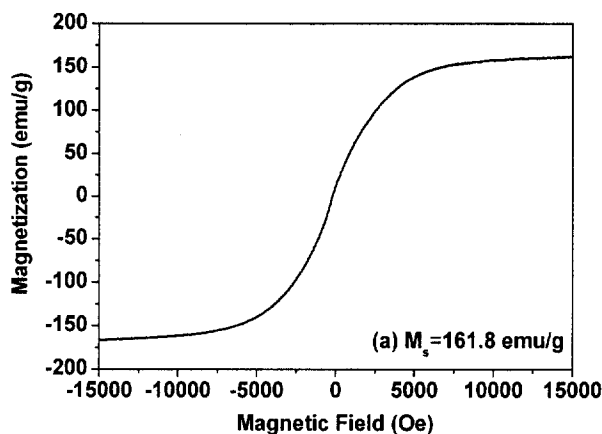


Figure 3-6. SEM-EDS data of Co nanoparticles.

3-1-1-5. VSM

The saturation magnetization (M_s) was measured at room temperature in a maximum applied field of 15 kOe. Fig. 3-7 shows the hysteresis loop of Co nanoparticle powder to characterize magnetic properties at room temperature. The M_s of Co bulk material in literature is 162.5 emu/g at room temperature. The values of M_s are (a) 161.8 emu/g, (b) 148 emu/g, (c) 151.2 emu/g and 170.3 emu/g. The M_s of hcp phase of cobalt particle was higher than that of fcc nanosized-cobalt particle. However, the M_s of Co

nanoparticles (Fig. 3-7 (c)) prepared in 1,2-propanediol was close to that of bulk Co materials, not decreasing value of M_s like in the previous studies.^{15,62} Moreover M_s value of Co particle annealed at 800 °C is The superparamagnetic behavior is documented by the hysteresis loop measured at room temperature as shown in Fig. 3-7. There is almost immeasurable coercivity for Co nanoparticles at room temperature, which is a very typical behavior for a soft magnet. This indicates that the Co particles are superparamagnetic and nanosized.



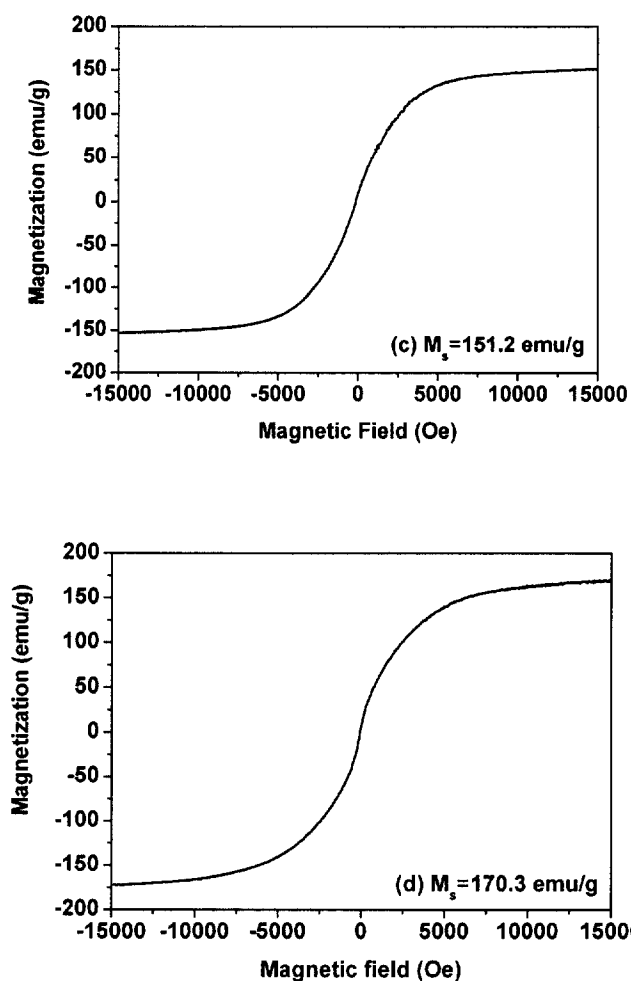


Figure 3-7. The hysteresis loops of Co nanoparticle according to different precursors. : (a) Co particle (precursor : $\text{Co}(\text{CH}_3\text{CO}_2)_2$ in ethylene glycol), (b) Co nanoparticle (precursor : $\text{Co}(\text{CH}_3\text{CO}_2)_2$ in 1,2-propanediol) and (c) Co nanoparticle (precursor : $\text{Co}(\text{OH})_2$ in 1,2-propanediol). (d) Co nanoparticle after annealed at 800 °C

3-1-2. Characterization of Co nanoparticle prepared by co-precipitation route

3-1-2-1. TEM image

TEM micrographs of Co nanoparticles (Fig. 3-8) were obtained. Co nanoparticles prepared by coprecipitation route has a less definitional image than thermal decomposition process. The size of Co nanoparticles was determined as 30~40 nm and shape is amorphous.

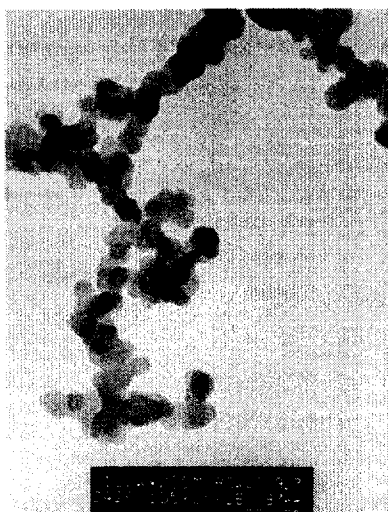


Figure 3-8. TEM image of Co nanoparticles.

3-1-2-2. XRD

Generally, XRD can be used to characterize the crystallinity of nanoparticle. The XRD patterns of the Co nanoparticle samples are shown in Fig. 3-9. The discernible peaks in Fig. 3-9 can be indexed to (100), (002), (101), (110) and (103) planes of a hexagonal unit cell, which corresponds to that of cobalt structure (JCPDS card no. 05-0727). This sample need to be annealed at high temperature to have crystallinity.

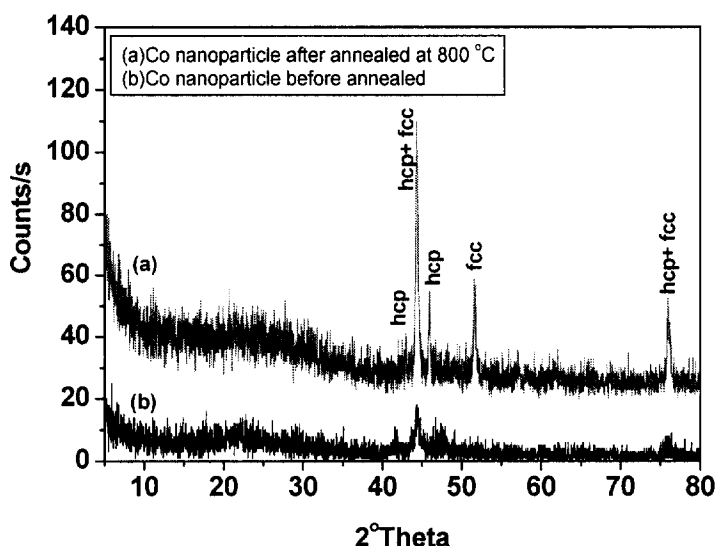


Figure 3-9. (a) XRD pattern of amorphous Co nanoparticles. (b) Co nanoparticle after annealed at 800 oC

3-1-2-3. EPMA

EPMA analysis (Fig. 3-10) was carried out for Co nanoparticles prepared by co-precipitation route to obtain contents of sample. Fig. 3-10 indicates in order the contents of Co and B are 98.157 : 1.843 as atm%. There is no impurity except cobalt and boron components. Washing product sufficiently is positively necessary to obtain pure product not including contents of Na^+ and Cl^- ions. In proportion to the increase of reaction time, the content of boron is on the increase and the product is oxidized gradually. We can present the mechanism of nanoparticles by the coprecipitation method as mentioned in the background section. Adding borohydride derivative excessively causes increase of boron content in the product. So sodium borohydride was added as the minimum quantity.

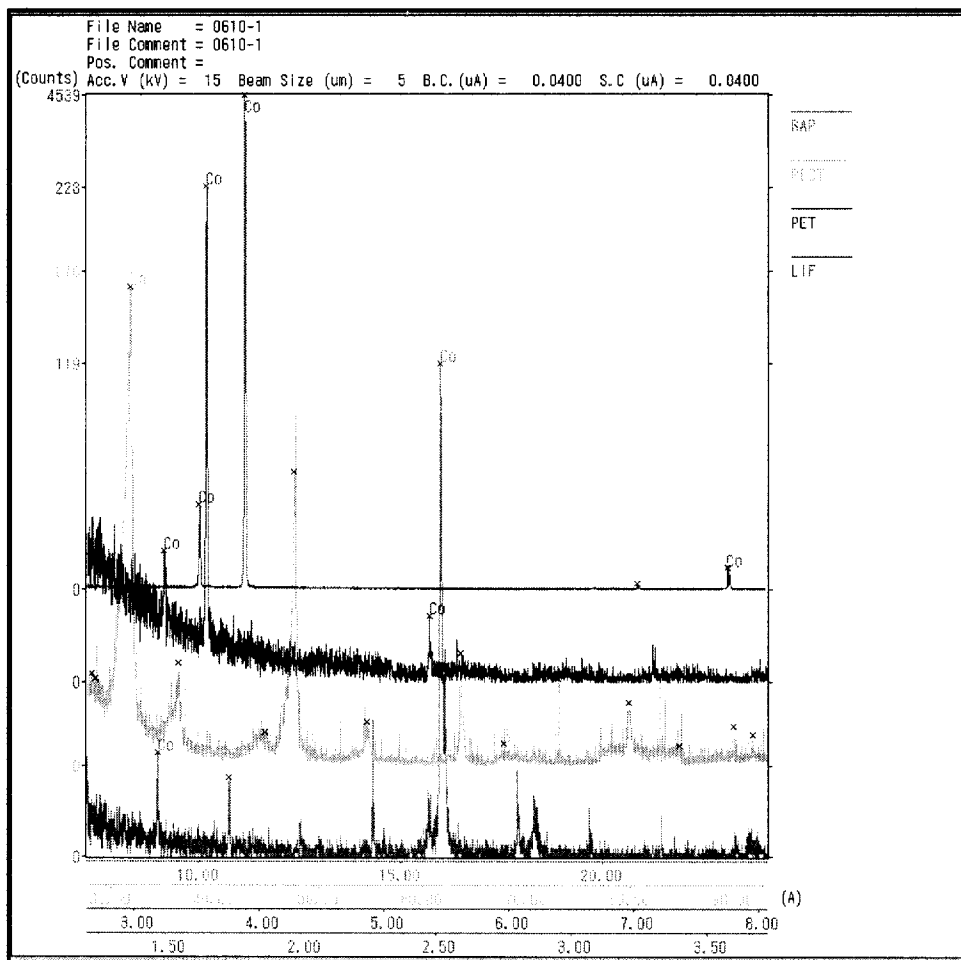


Figure 3-10. EPMA graphs of Co nanoparticles prepared by coprecipitation route.

3-1-2-4. SQUID

The saturation magnetization (M_s) of magnetic nanoparticles have been determined by using superconducting quantum interference device with maximum applied field of 50 kOe. Fig. 3-11 shows hysteresis loop of Co nanoparticle powder to characterize magnetic properties at room temperature. The values of M_s and coercivity were 68.86 emu/g and 454 Oe, respectively.

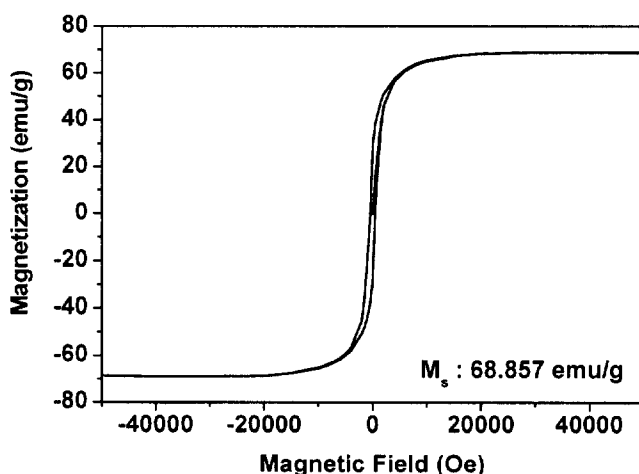


Figure 3-11. The hysteresis loop of the Co nanoparticle.

3-1-3. Characterization of Co nanoparticle prepared by solventless thermal decomposition

3-1-3-1. TGA

We prepared Co nanoparticles by new solventless thermal decomposition. The thermal decomposition temperature of the Co^{2+} -oleate₂ complex was studied by TGA analysis (Fig. 3-12). The sample was heated from 50 °C to 700 °C. Fig. 3-12 shows the weight loss for Co^{2+} -oleate₂ complex by heating under nitrogen gas. A strong endothermic peak for Co^{2+} -oleate₂ complex was obtained at 439 °C. The peak indicates the decomposition of oleate molecule of Co^{2+} -oleate₂ complex according to the increase of temperature.

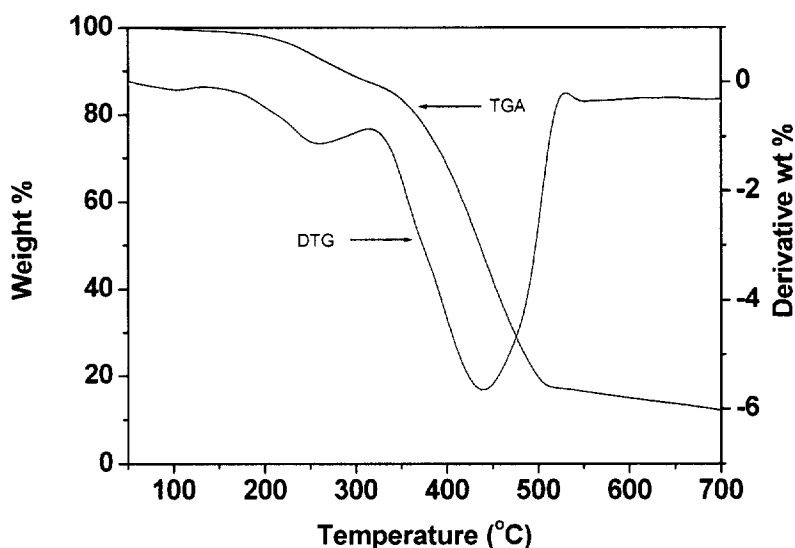


Figure 3-12. Thermogravimetric analysis data for Co^{2+} -oleate₂ complex during heat treatment.

3-1-3-2. TEM

TEM micrographs of Co nanoparticles (Fig. 3-13) were obtained. TEM sample was prepared when a drop of the nanoparticle in iso-octane solution was carefully placed on the grid and dried in air. The sizes of Co nanoparticles were determined as about 44 nm. Most of the Co nanoparticles are spherical. In this process, in spite of high temperature the particle was obtained as nanosize.

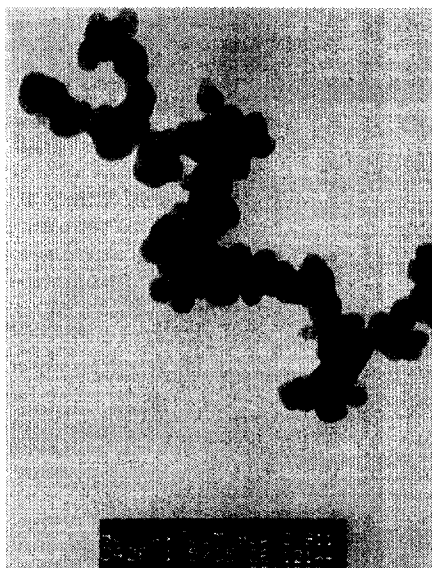


Figure 3-13. TEM image of Co nanoparticles synthesized by thermal decomposition.

3-1-3-3. XRD

The XRD patterns of the Co nanoparticle samples are shown in Fig. 3-14. The discernible peaks in Fig. 3-14 can be indexed to (100), (002), (101), (110) and (103) planes of a hexagonal unit cell, which corresponds to that of cobalt structure (JCPDS card no. 05-0727). This sample has high crystallinity at the reaction temperature compared with the Co nanoparticles that was prepared with co-precipitation route.

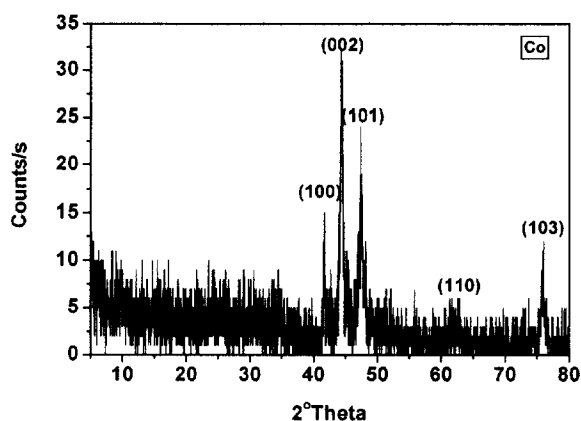


Figure 3-14. X-ray diffractogram of Co nanoparticles.

3-1-3-4. FE-SEM

FE-SEM micrographs are revealing the particle size and morphology of the Co nanoparticles as Fig. 3-15 (a) and (b). The average particles size of Co nanoparticle was determined to be about 1 μm (Fig. 3-15 (a) and (b)). The Co grains were observed as about 60 nm. The unstable nanoparticle is aggregated to micron sized particles.

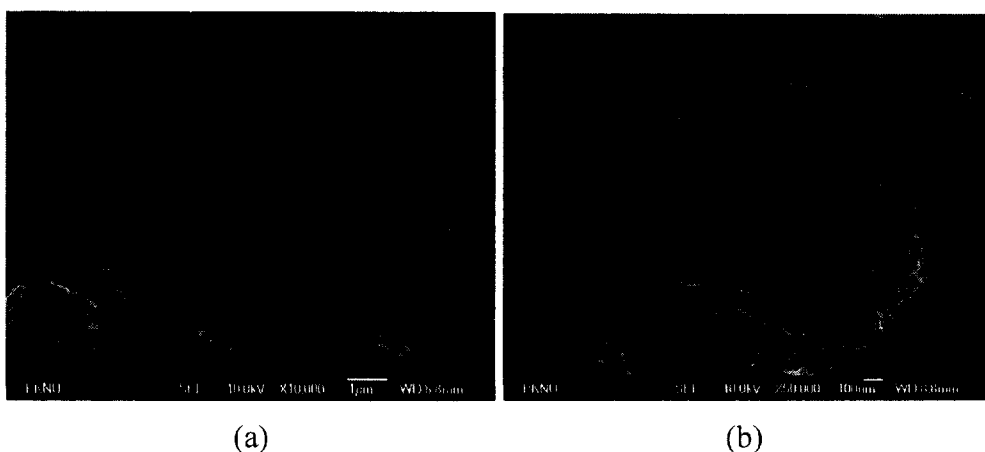


Figure 3-15. FE-SEM micrographs of Co nanoparticles synthesized by

thermal decomposition. : (a) magnitude of $\times 10,000$ and (b) magnitude of $\times 10,000$.

3-1-3-5. SEM-EDS

SEM-EDS analysis (Fig. 3-16) was carried out for Co nanoparticle by electron beams (200 kV) to investigate the contents of our sample. EDX data of Fig. 3-16 indicates 100% of cobalt. Fig. 3-16 indicates that there is no impurity except the cobalt component. Washing the product sufficiently is necessary to obtain pure product to remove Na^+ and Cl^- ions.

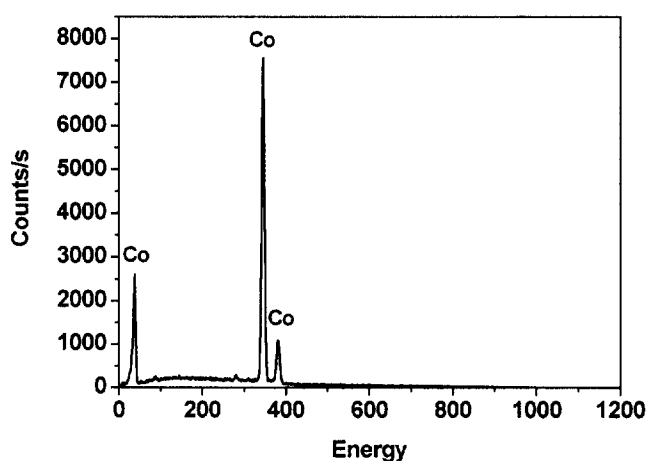


Figure 3-16. SEM-EDX of Co nanoparticles.

3-1-3-6. VSM

The saturation magnetization (M_s) was measured at room temperature in a maximum applied field of 15 kOe. Fig. 3-17 shows the hysteresis loop of Co nanoparticle powder to characterize magnetic properties at room temperature. The value of saturation magnetization and coercivity are 165.43 emu/g of Co nanoparticle.

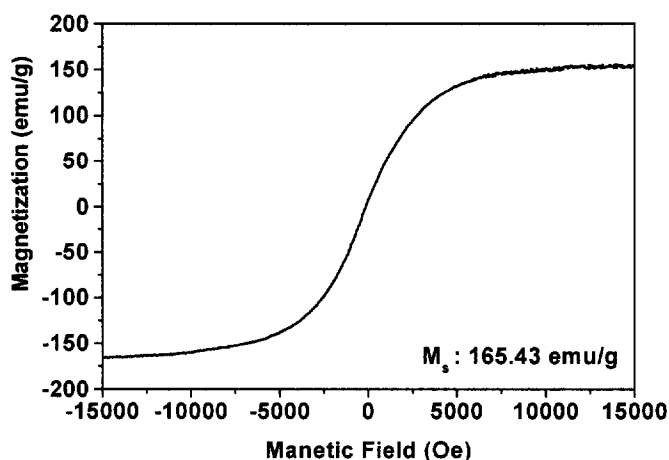


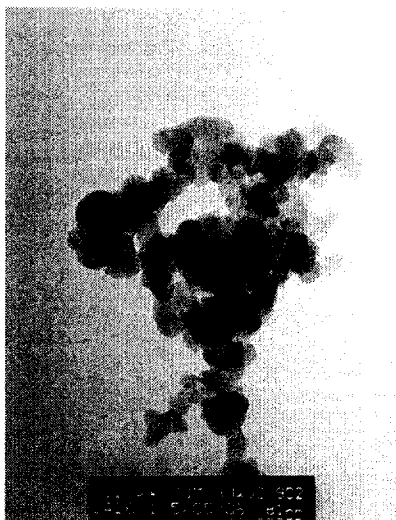
Figure 3-17. The hysteresis loop of the Co nanoparticle.

3-2. Preparation of FeCo nanoparticle

3-2-1. Characterization of FeCo nanoparticle synthesized by coprecipitation route

3-2-1-1. TEM

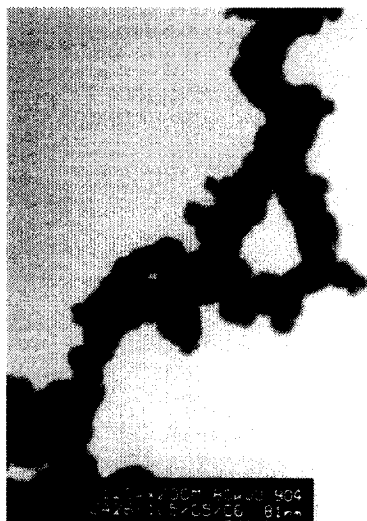
TEM micrographs of FeCo nanoparticles (Fig. 3-18) were compared according to different reaction times. TEM samples were formed when a drop of the nanoparticles in iso-octane solution was carefully placed on the grid and dried in air. As we can see, FeCo nanoparticle that was prepared by the reaction for 4 hrs has definitional image and uniform size. The size of FeCo nanoparticles was about 35 nm. As the reaction time is getting longer, it has low definitional image. The FeCo nanoparticle (Fig. 3-18 (c)) with reaction time of 8 hrs was aggregated partially, as shown in Fig. 3-18(c).



(a)



(b)

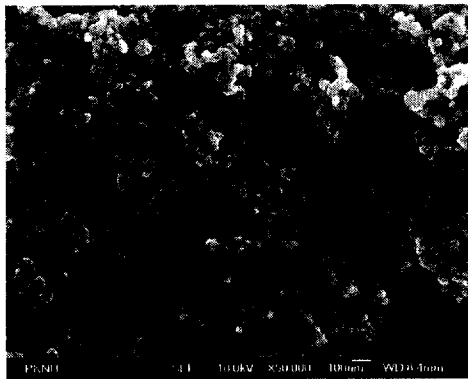


(c)

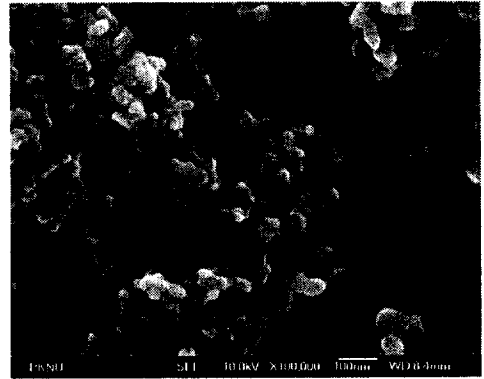
Figure 3-18. The TEM images of FeCo nanoparticle : (a) FeCo nanoparticle synthesized for 1 hr, (b) FeCo nanoparticle synthesized for 4 hrs and (c) FeCo nanoparticle synthesized for 8 hrs.

3-2-1-2. FE-SEM

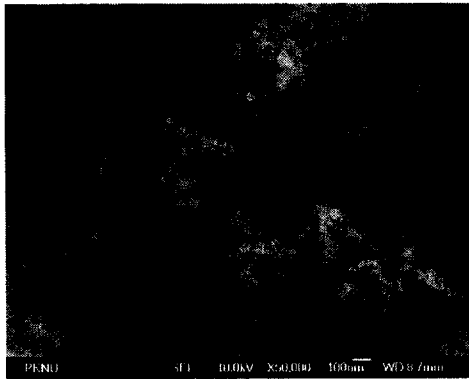
The morphology of FeCo nanoparticles was characterized by FE-SEM images. The uniform grain size depends on the stirring speed and reaction time. Fig. 3-19 shows FE-SEM images of FeCo nanoparticles that was prepared for 1 hr, 4 hrs and 8 hrs, respectively. As reaction time increase, the particle has uniform size and shape (Fig. 3-19 (c) and (d)). But the longer reaction time is, the more aggregated the particle was (Fig. 3-19 (e) and (f)).



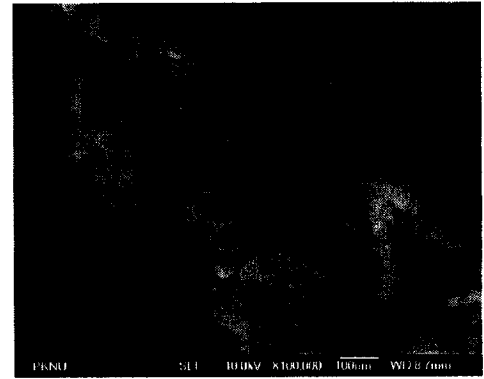
(a)



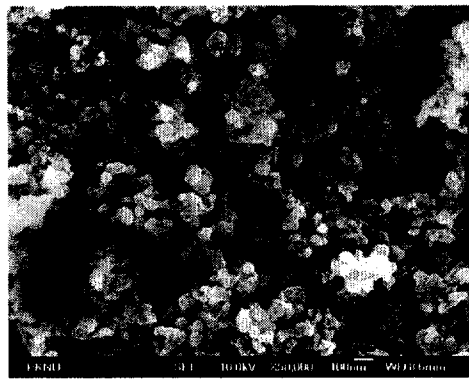
(b)



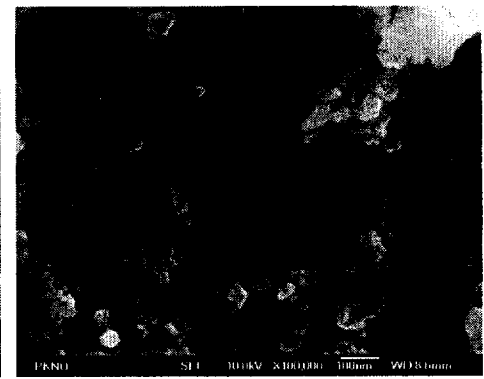
(c)



(d)



(e)



(f)

Figure 3-19. FE-SEM images of FeCo nanoparticle according to different reaction times : (a) FeCo nanoparticle : 1 hr (x50,000), (b)

FeCo nanoparticle : 1 hr (x100,000), (c) FeCo nanoparticle : 4 hrs (x50,000), (d) FeCo nanoparticle : 4 hrs (x100,000), (e) FeCo nanoparticle : 8 hrs (x50,000) and (f) FeCo nanoparticle : 8 hrs (x100,000).

3-2-1-3. XRD

Usually nanoparticle that was prepared by coprecipitation route has amorphous phase. Fig. 3-20 shows the XRD patterns of amorphous FeCo nanoparticle and FeCo nanocrystallite after annealed at 800 °C for 1 hr. The XRD pattern of Fig. 3-20 (a) has a main peak at $2\theta = 44.87026$, corresponding to the (110) planes of a cubic unit cell (JCPDS card no. 48-1816). In Fig. 3-19 (b), the peaks can be indexed to (110), (200) and (211).

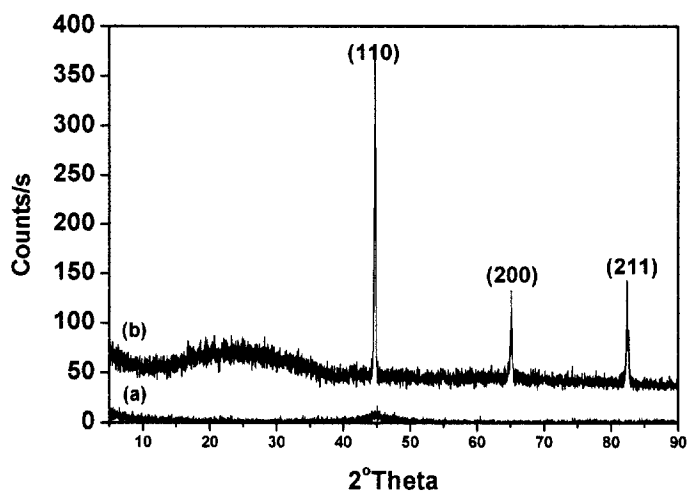
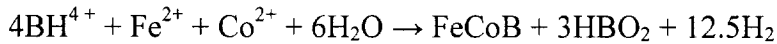
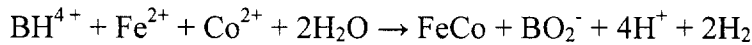
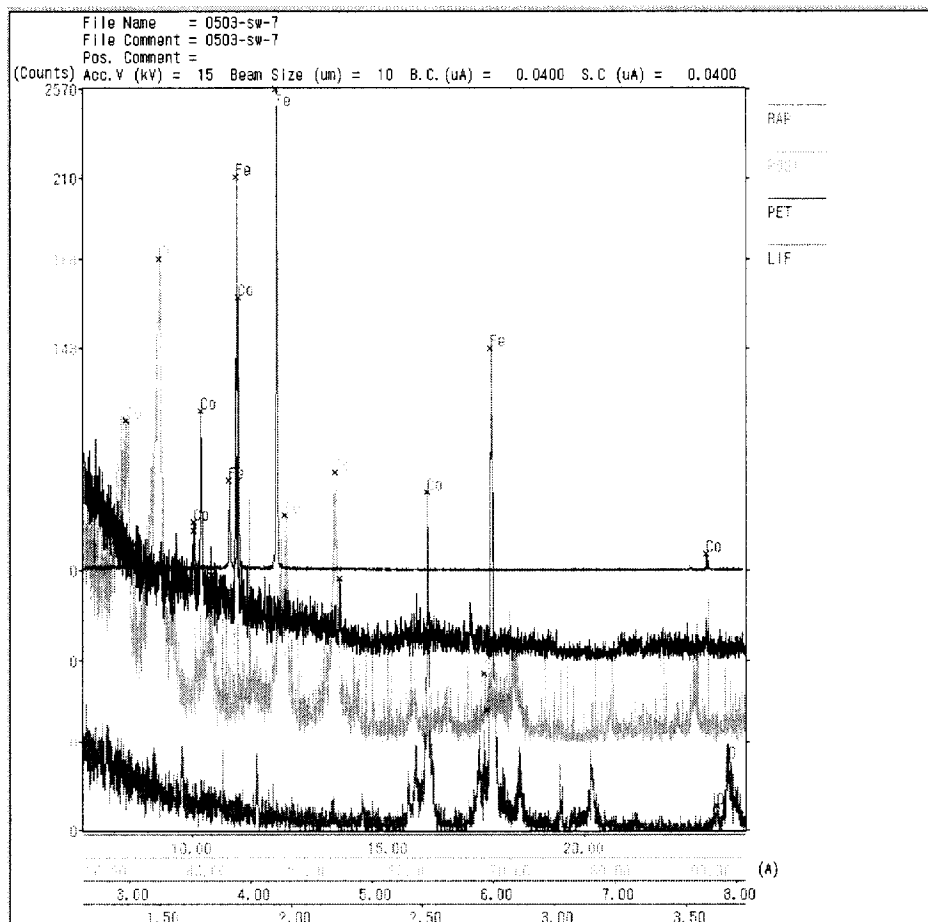


Figure 3-20. XRD patterns of FeCo nanoparticles.: (a) amorphous FeCo nanoparticle and (b) FeCo nanoparticle annealed at 800 °C for 1 hr.

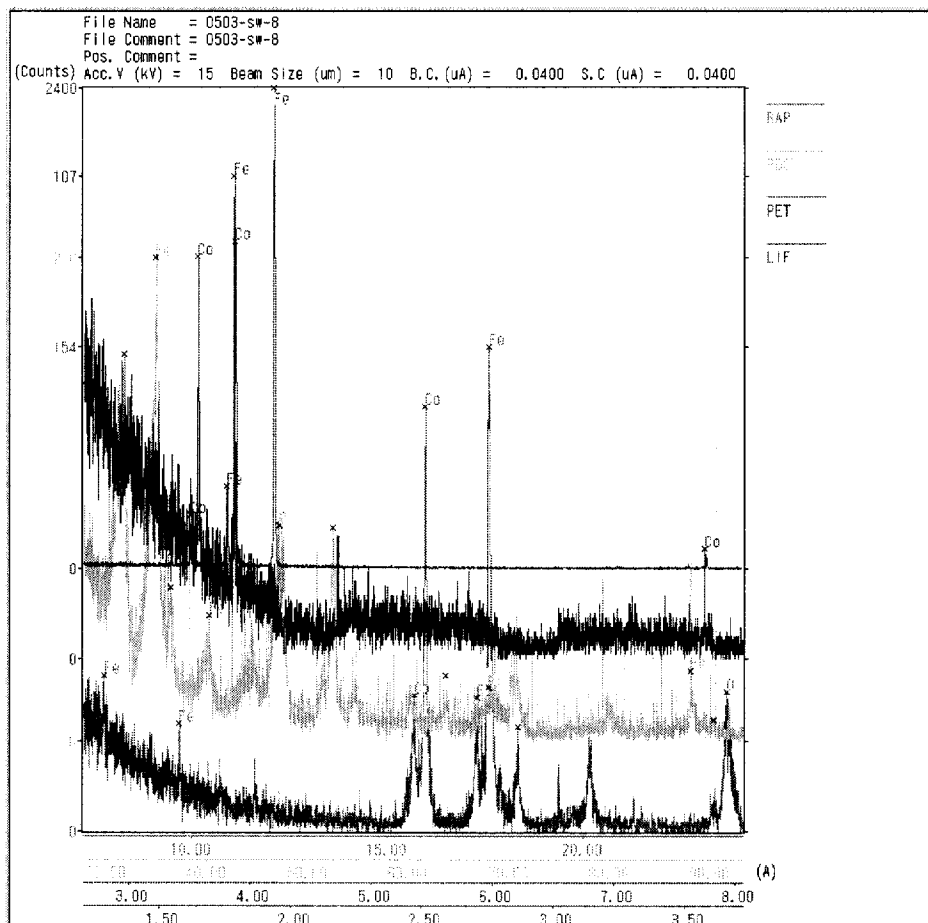
3-2-1-4. EPMA

EPMA analysis (Fig. 3-21) was carried out for the FeCo nanoparticle to obtain contents of sample. Fig. 3-21 indicates in order the contents of Fe, Co, O and B are (a) 0.5495 : 0.4061 : 0.0163 : 0.028 (b) 0.5012 : 0.2918 : 0.1775 : 0.0295 (c) 0.3307 : 0.2309 : 0.3502 : 0.0883. There is no impurity except cobalt, iron, boron, oxygen components. Washing the product sufficiently is positively necessary to obtain pure product not including contents of Na⁺ and Cl⁻ ions. In proportion to the increase of reaction time, content of boron is on the increase and product is oxidized gradually. We can present two mechanism of FeCo nanoparticle by coprecipitation method as follows⁴⁷. Adding the borohydride derivative excessively causes an increase of boron content in the product. So the amount of sodium borohydride was reduced to the minimum.





(b)



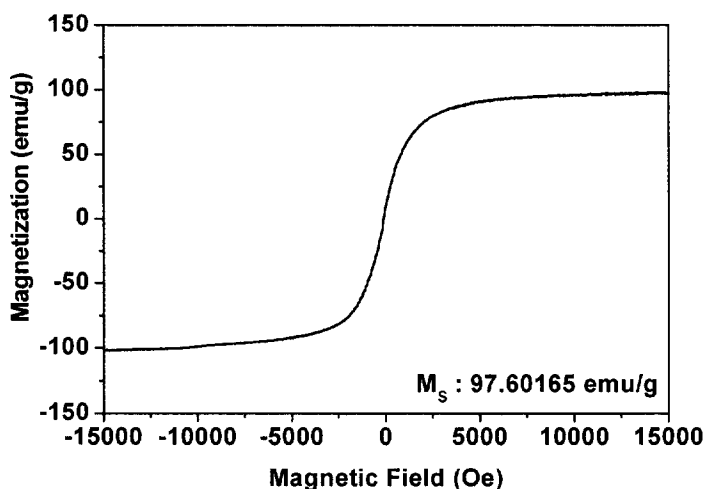
(c)

Figure 3-21. EPMA data of FeCo nanoparticles : (a) FeCo nanoparticle synthesized for 1 hr, (b) FeCo nanoparticle synthesized for 4 hrs and (c) FeCo nanoparticle synthesized for 8 hrs.

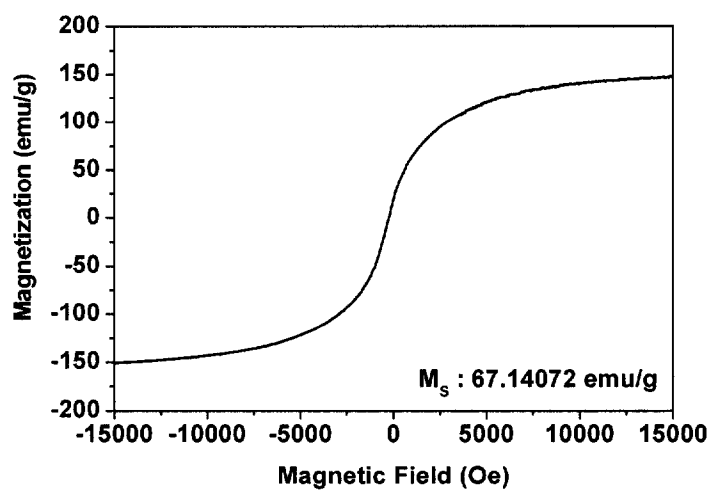
3-2-1-5. VSM

The saturation magnetization (M_s) of the magnetic nanoparticle has been determined by using vibrating sample magnetometer with maximum applied field of 15 kOe. Fig. 3-22 shows hysteresis loop of FeCo nanoparticle powders to characterize magnetic properties at room temperature. The

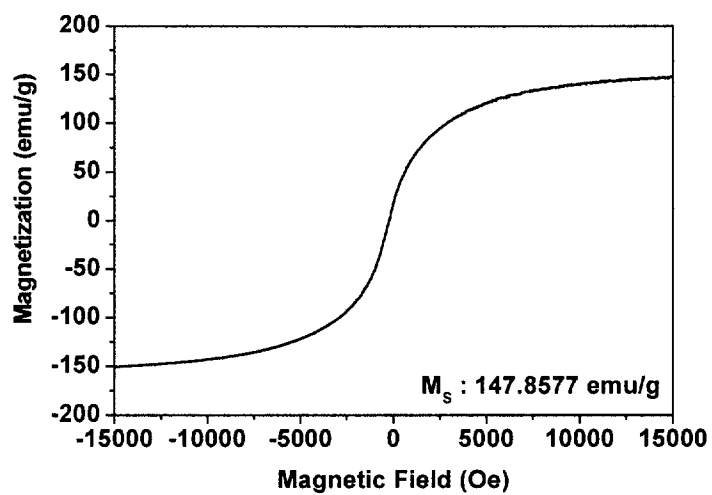
values of M_s was (a) 97.60165 emu/g, (b) 147.8577 emu/g, (c) 67.14072 emu/g. The value of M_s of FeCo nanoparticles prepared for 4 hrs was the highest in this study. It means it needs enough time to be nucleated when the metal ion is reduced into metal. However, excess reaction time causes low M_s . The optimum time was fixed for 4 hrs. As the particle size is increased, the magnetic transport takes place from superparamagnetic to ferromagnetic. As reaction time becomes longer, the remanence magnetization (M_r) is increased. In Fig. 3-22 (d), after amorphous FeCo nanoparticle annealed at 800 °C for 1 hr, the value of M_s (182 emu/g) was increased, positively.



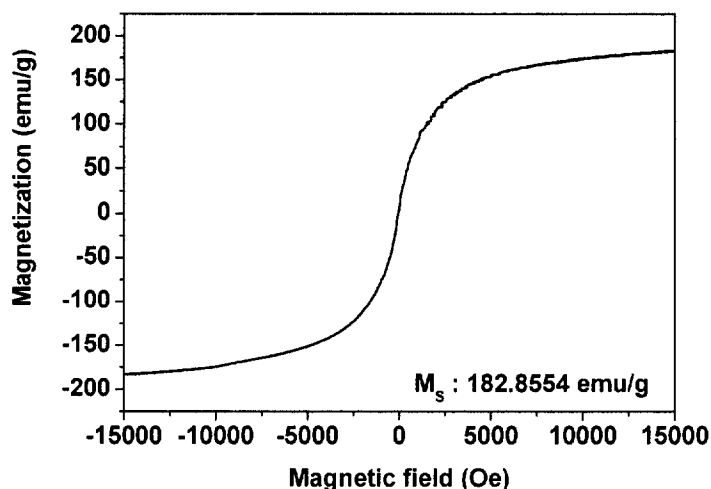
(a)



(b)



(c)



(d)

Figure 3-22. The hysteresis loops of the FeCo nanoparticle : (a) FeCo nanoparticle synthesized for 1 hr, (b) FeCo nanoparticle synthesized for 4 hrs, (c) FeCo nanoparticle synthesized for 8 hrs and (d) FeCo nanoparticle after annealed at 800 °C for 1 hr.

3-2-2. Characterization of FeCo nanoparticle synthesized by polyol method

3-2-2-1. TEM

Fig. 3-23 shows low-resolution TEM images of FeCo nanoparticle synthesized by polyol process. Fig. 3-23 is the FeCo nanoparticle synthesized with the surfactant. The nanoparticles need to be coated with organic surfactants to prevent them from irreversible aggregation. Oleic acid was widely used in the synthesis of metal nanoparticles. The size of the FeCo nanoparticles was about 40 nm. And the size of FeCo nanoparticle

synthesized with oleic acid was about 10 nm. Fig. 3-23 (c) shows TEM lattice image for one particle indicating highly crystalline structure. Co lattice spacing of 1.25 Å was consistent with the lattice spacing of (210) plane of FeCo crystal structure. That means that FeCo nanoparticle is formed as single domain.

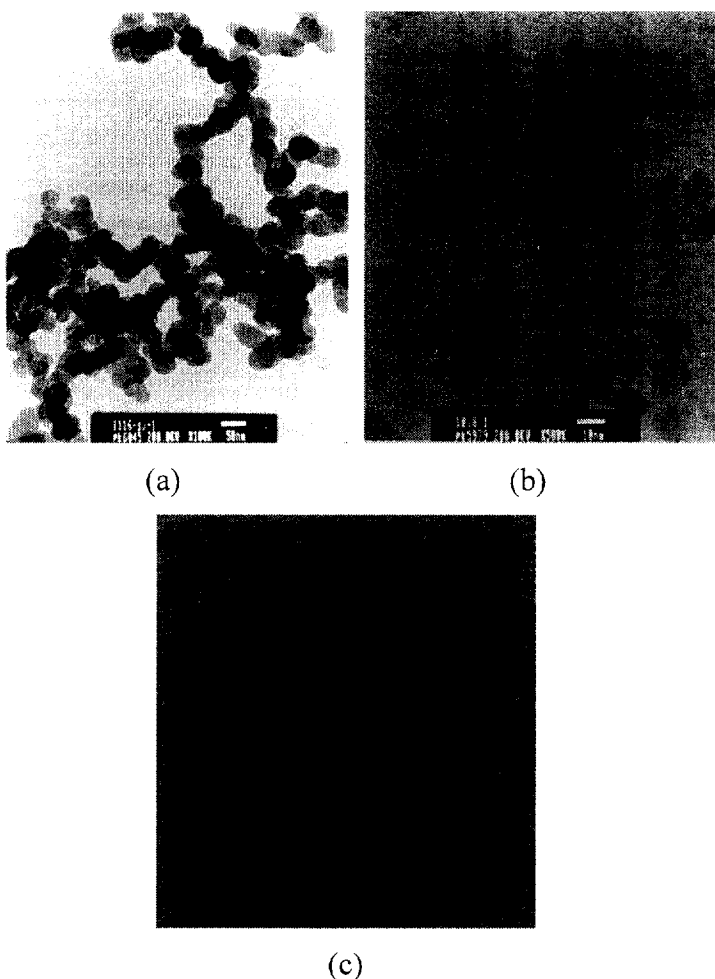
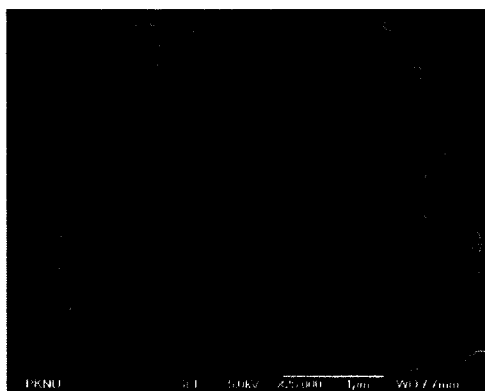


Figure 3-23. (a) TEM image of FeCo nanoparticles and (b) Size controlled FeCo nanoparticle (c) HR-TEM image of FeCo nanocrystallite single domain.

3-2-2-2. FE-SEM

The morphology of the FeCo nanoparticle was characterized by FE-SEM images (Fig. 3-24). The grain size for the nanoparticle was controlled according to presence of stabilizing surfactant of oleic acid and different solvent. When oleic acid was not added, the grain size was about from 500 nm to 1 μ m. On the other hand, when the surfactant as stabilizer was added, the reduced size was confirmed and the particle size was uniformly distributed. When metal ion is nucleated, metal particle nucleated already is surrounded by oleic acid. Then particle size can be controlled. Solvent, too, influences over controlling particle size. After metal ion is nucleated, the particle is surrounded with the lone pair electron of oxygen of 2,3-butanedione as surfactant. When trimethylene glycol is used instead of ethylene glycol as solvent, 3,4-hexanedione is formed. It causes that space between particles is expanded. Then the particle size is regulated.



(a)

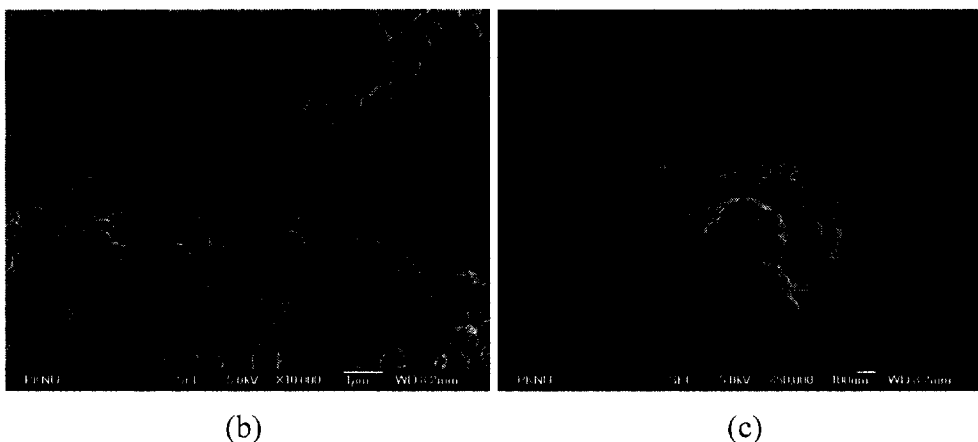


Figure 3-24. FE-SEM images of FeCo nanoparticles : (a) before the size of FeCo nanoparticle is controlled (x25,000), (b) after the size of FeCo nanoparticle is controlled (x10,000), (c) after the size of FeCo nanoparticle is controlled (x50,000).

3-2-2-3. XRD

Fig. 3-25 shows the XRD patterns of the FeCo nanoparticle. The crystal structure of FeCo nanoparticle has been confirmed as the bcc phase. The XRD pattern has three main peaks at $2\theta = 44.828, 55.678, 65.263, 74.153$ corresponding to the (110), (111), (200), (210) as compared with JCPDS card no. 44-1433. As we can see, the FeCo nanoparticle prepared by the polyol method has more crystalline than those prepared by the coprecipitation route.

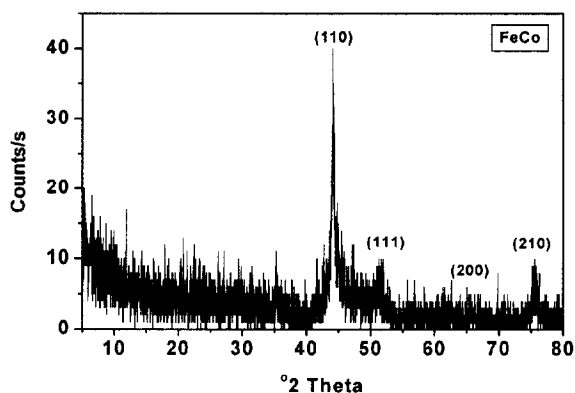


Figure 3-25. XRD pattern of FeCo nanoparticles.

3-2-2-4. SEM-EDS

SEM-EDS analysis (Fig. 3-26) was carried out for FeCo nanoparticle to obtain contents of sample. Fig. 3-26 indicates the contents of Fe and Co are 16.79%, 83.21%, respectively. There is no impurity except cobalt and iron components. Washing the product sufficiently is absolutely necessary to obtain pure product not including contents of Na^+ and Cl^- ions.

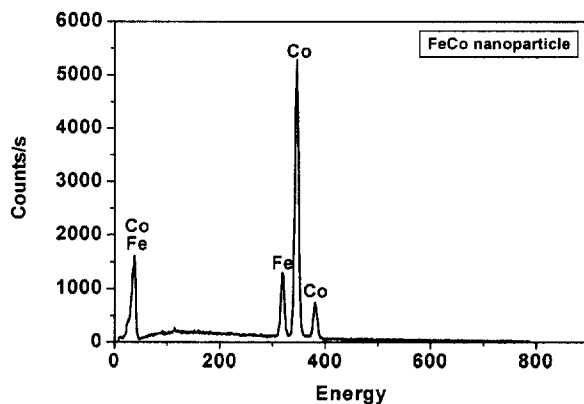


Figure 3-26. SEM-EDS data of FeCo nanoparticles.

3-2-2-5. VSM

The saturation magnetization (M_s) of magnetic nanoparticle has been determined by using vibrating sample magnetometer with maximum applied field of 15 kOe. Fig. 3-27 shows hysteresis loop of the FeCo nanoparticle powder to characterize magnetic properties at room temperature. The saturation magnetization (M_s) was determined as 176.01 emu/g. The value of M_s of FeCo nanoparticles prepared from polyol method under presence of surfactant was the highest in this study. There is immeasurable coercivity for FeCo nanoparticles at room temperature, which is a very typical behavior for a soft phase magnet. This means that FeCo nanoparticles are superparamagnetic and nanosized.

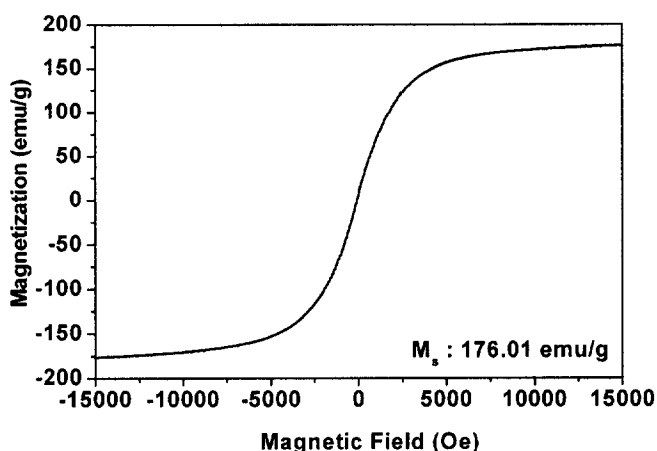


Figure 3-27. The hysteresis loop of the FeCo nanoparticle.

3-3. Preparation of CoFe_2O_4 nanoparticle

3-3-1. Characterization of CoFe_2O_4 nanoparticle synthesized by polyol method

3-3-1-1. XRD

Fig. 3-28 shows the XRD pattern of the CoFe_2O_4 nanoparticle samples. The diffraction peaks can be indexed to (220), (311), (400), (422), (511) and (440) planes of cubic unit cell, corresponding to JCPDS card no. 22-1086. No other peak of impurities is not detected. The crystal size determined by Debye-Sherre equation with XRD data is 16.2 nm, which is close to the particle sizes calculated from TEM images. This indicates that CoFe_2O_4 are all nanocrystalline.

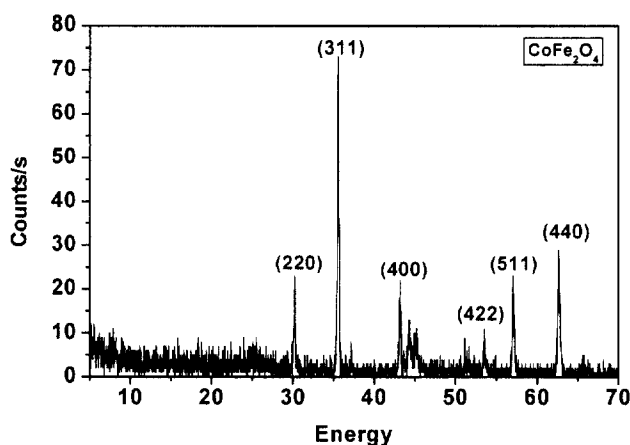
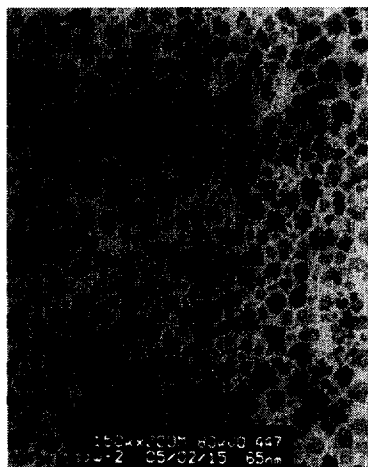


Figure 3-28. XRD pattern of CoFe_2O_4 nanoparticles.

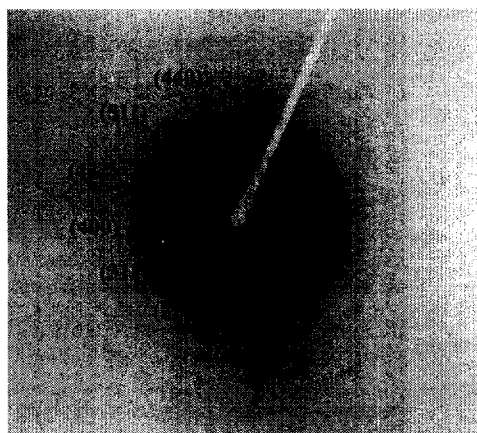
3-3-1-2. TEM

Fig. 3-29 shows low-resolution TEM images of monodispersed CoFe_2O_4 nanoparticles. TEM samples were formed when a drop of the nanoparticle in iso-octane solution was carefully placed on the grid and dried in air. In Fig. 3-29 (a) the size of CoFe_2O_4 nanoparticle prepared polyol process was about 10~15 nm. Fig. 3-29 shows the electron

diffraction pattern exhibited a CoFe_2O_4 crystal structure. The diffraction rings can be indexed to (220), (311), (400), (422), (511) and (440) planes at CoFe_2O_4 nanocrystallite. The same result is observed for XRD spectra of Fig. 3-28. This indicates that the nanocrystallites in TEM is CoFe_2O_4 nanoparticle.



(a)



(b)

Figure 3-29. (a) The low-resolution TEM image of CoFe_2O_4 nanoparticles and (b) ED pattern of CoFe_2O_4 nanoparticles.

3-3-1-3. SEM-EDS

SEM-EDS analysis (Fig. 3-30) was carried out for the CoFe_2O_4 nanoparticles to obtain contents of sample. Fig. 3-30 indicates in order the contents of Fe, Co and O are 40.36%, 41.72%, and 17.92%. There is no impurity except cobalt, iron and oxygen components. Washing product sufficiently is absolutely necessary to obtain pure product not including contents of Na^+ and Cl^- ions.

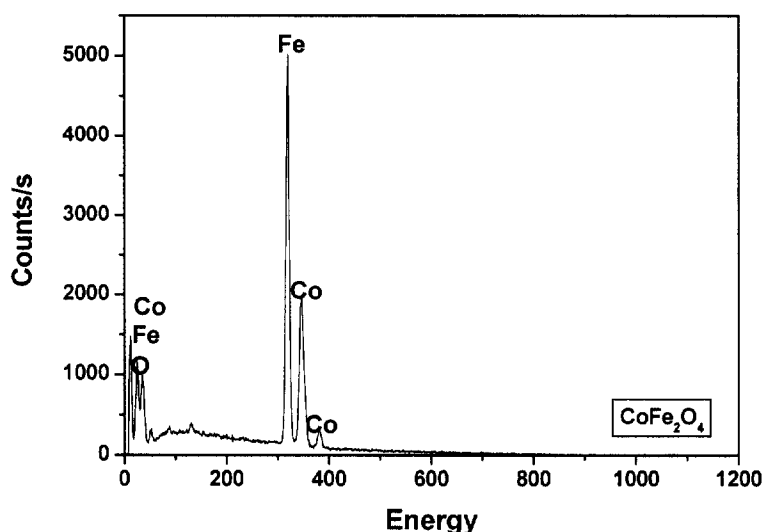


Figure 3-30. SEM-EDS data of CoFe_2O_4 nanoparticles.

3-3-1-4. FE-SEM

The morphology of the CoFe_2O_4 nanoparticle was characterized by FE-SEM images. The uniform grain size depends on stirring speed and reaction time. Fig. 3-31 shows FE-SEM images of the CoFe_2O_4 nanoparticles.

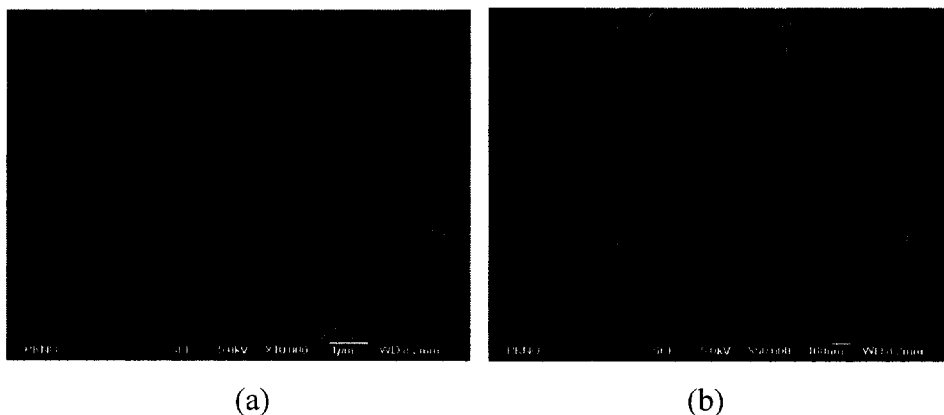


Figure 3-31. FE-SEM images of CoFe_2O_4 nanoparticles : (a) with magnitude of $\times 10,000$ and (b) with magnitude of $\times 50,000$.

3-3-1-5. SQUID

The saturation magnetization (M_s) of magnetic nanoparticle have been determined by using superconducting quantum interference device with maximum applied field of 50 kOe. Fig. 3-32 shows hysteresis loop of the CoFe_2O_4 nanoparticle to characterize magnetic properties at room temperature. The saturation magnetization (M_s) and coercivity were 65.14 emu/g and 449 Oe, respectively.

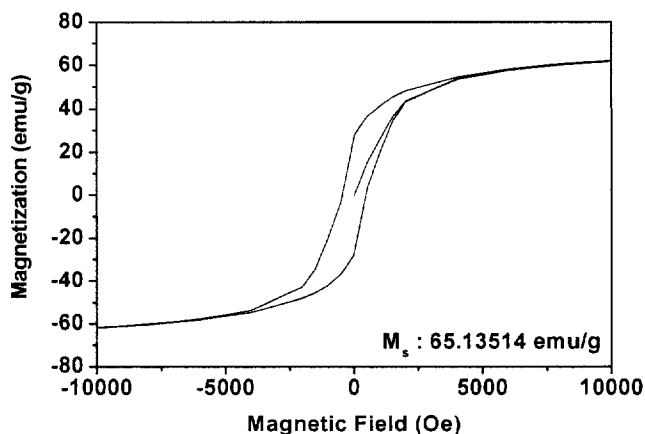


Figure 3-32. The hysteresis loop of CoFe₂O₄ nanoparticle.

3-4. Preparation of SmCo nanoparticles

3-4-1. Characterization of SmCo nanoparticle synthesized by solventless thermal decomposition.

3-4-1-1. TGA

The thermal decomposition temperature of the mixture of the Sm²⁺-oleate₂ and Co²⁺-oleate₂ complexes was studied by TGA analysis. The sample was heated from 50 °C to 800 °C. Fig. 3-33 shows the thermogravimetric analysis data for the mixture of the Sm²⁺-oleate₂ and Co²⁺-oleate₂ complexes by heating under nitrogen gas. A strong endothermic peak for the mixture of the Sm²⁺-oleate₂ and Co²⁺-oleate₂ complexes was obtained at 413 °C and 471 °C. The peak indicates the decomposition of oleate molecule of the mixture of the Sm²⁺-oleate₂ and Co²⁺-oleate₂ complexes according to the increase of temperature. The annealing temperature was executed at 400 °C,

450 °C and 500 °C.

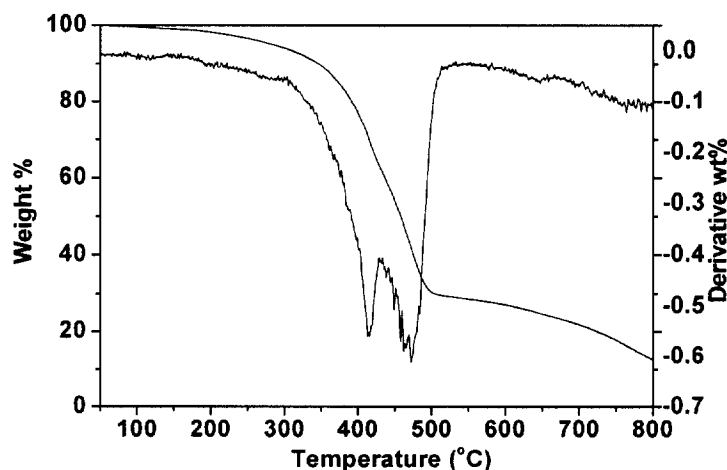


Figure 3-33. Thermogravimetric analysis data for the mixture of the Sm^{2+} -oleate₂ and Co^{2+} -oleate₂ complexes during heat treatment.

3-4-1-2. TEM

TEM micrographs of the SmCo nanoparticles (Fig. 3-34) were obtained with different amounts of Sm and Co contents. The TEM samples were prepared when a drop of nanoparticles with different the molar ratio of Sm to Co contents (a) SmCo nanoparticle (Sm : 2.32%) (b) SmCo nanoparticle (Sm : 13.54%), (c) SmCo nanoparticle (Sm : 17.80%). The nanoparticle in iso-octane solution was carefully placed on the grid and dried in air. The sizes of SmCo nanoparticles were determined as about (a) 44 nm (b) 40 nm and (c) 43 nm. Most of the SmCo nanoparticles are spherical. In the previous report, to prepare SmCo particle, the particles have been fabricated with various kinds of methods like sintered magnet, sputtered magnet, magnet by HDDR process and so on⁶⁴⁻⁶⁷. In those processes, it has a difficulty in obtaining the magnetic nanosized-particles.

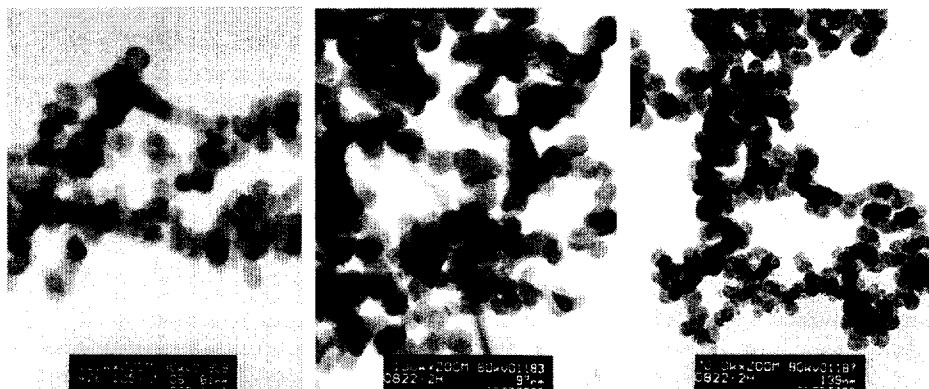


Figure 3-34. TEM images of (a) SmCo nanoparticle (Sm : 2.32%), SmCo nanoparticle (b) (Sm : 13.54%) and (c) SmCo (Sm : 17.80%) nanoparticle synthesized by thermal decomposition.

3-4-1-3. XRD

The Co component was more reducible itself easily by thermal decomposition than Sm components. Due to this reason, a strong Co peak was detected in all samples. Although absolute intensity of all the peaks of Co was higher than the peak of the SmCo nanoparticles; as Sm content increases, the peak of the SmCo nanoparticles is shown definitely.

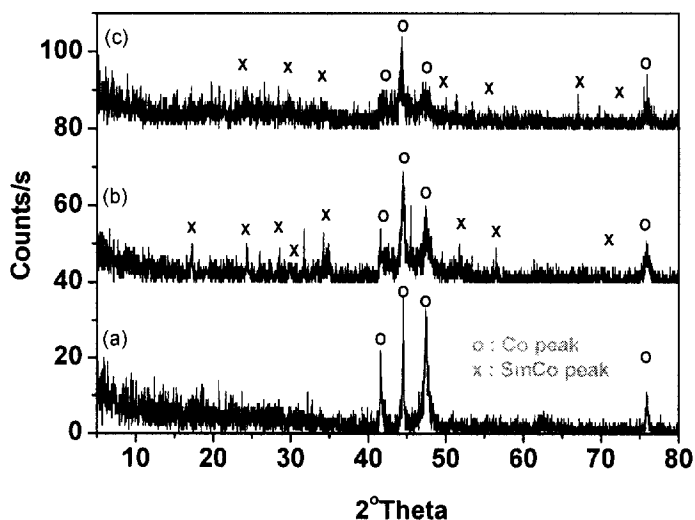


Figure 3-35. X-ray diffractograms of SmCo nanoparticles with different amounts of Sm and Co contents : (a) SmCo nanoparticles (Sm : 2.32%), (b) SmCo nanoparticles (Sm : 13.54%) and (c) SmCo nanoparticles (Sm : 17.80%).

3-4-1-4. FE-SEM

FE-SEM micrographs reveal the particle size and morphology of SmCo nanoparticles as Fig. 3-36 and Fig. 3-37, which explain about morphology according to reaction temperature. The mixture of the Sm^{2+} -oleate₂ and Co^{2+} -oleate₂ complexes was annealed at 400 °C (Fig. 3-37 (a)-(f)), 450 °C (Fig. 3-36 (a) and (b)) and 500 °C (Fig.3-36 (c) and (d)). In Fig. 3-36, as we can see, oleate is transformed. It has difficulty to separate nanoparticles. Moreover, low annealing temperature causes synthesis of SmCo nanoparticle that has low Sm content. So this experiment was carried out at 400 °C, as optimum temperature. The increase in SmCo particle size with the increasing Sm content is quite obvious in the micrographs (Fig. 3-37

(a)-(f). This value should be also compared with the average grain size for SmCo magnetic particles of ~ 10 nm in the previous study⁶⁸.

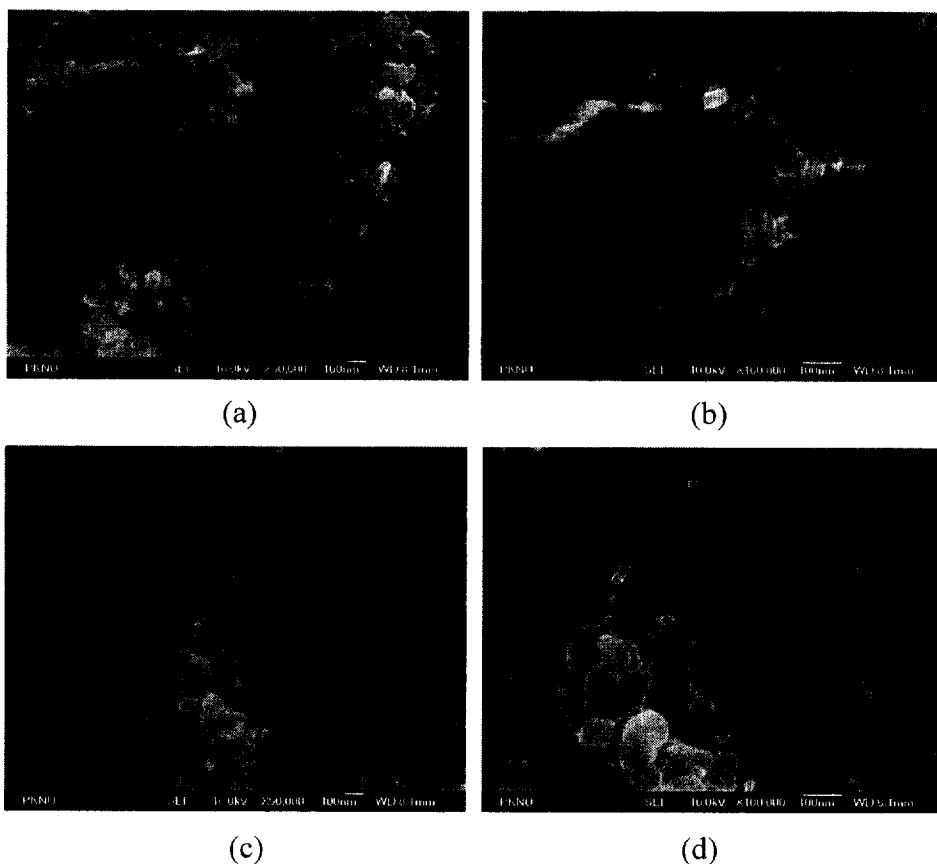
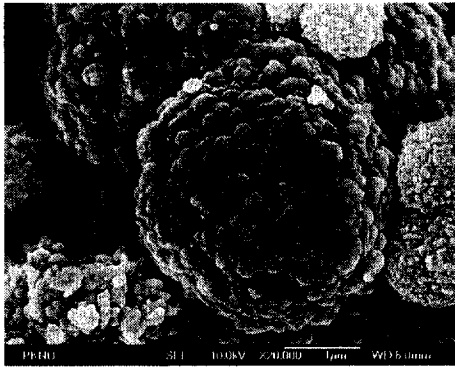
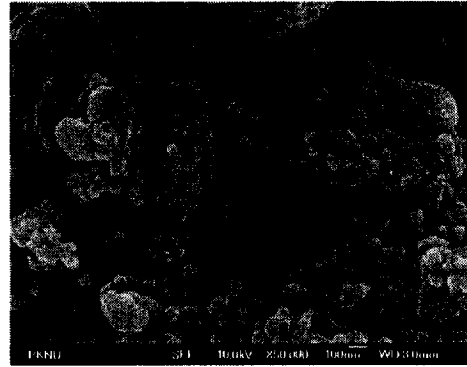


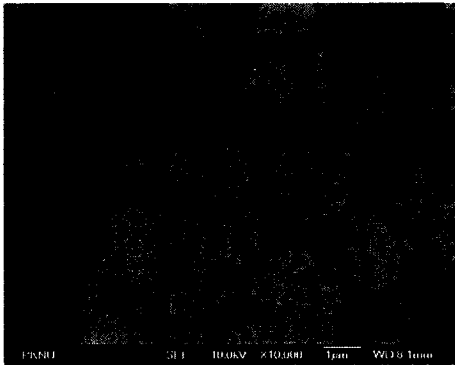
Figure 3-36. FE-SEM images of SmCo nanoparticle according to annealing temperature : (a) SmCo nanoparticle annealed at 450 °C (x50,000), (b) SmCo nanoparticle annealed at 450 °C (x100,000), (c) SmCo nanoparticle annealed at 500 °C (x50,000) and (d) SmCo nanoparticle annealed at 500 °C (x100,000).



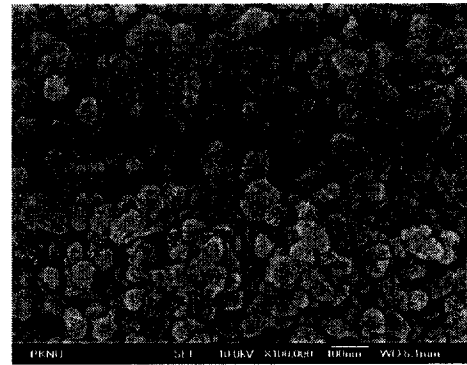
(a)



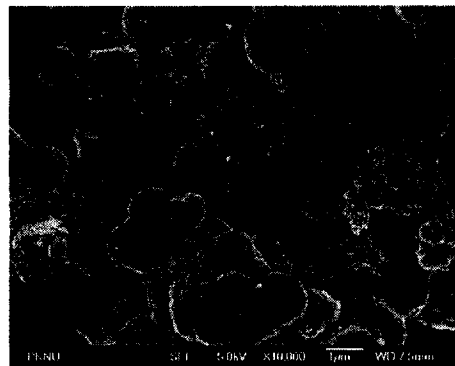
(b)



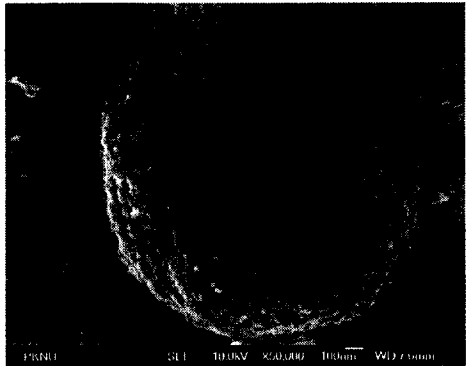
(c)



(d)



(e)



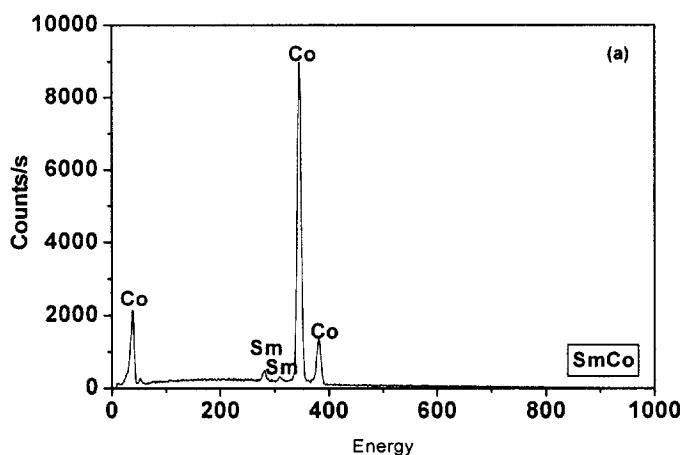
(f)

Figure 3-37. FE-SEM images of SmCo nanoparticle according to the molar ratio of Sm to Co : (a) SmCo nanoparticles (Sm: 2.32%)

(x20,000), (b) SmCo nanoparticles (Sm: 2.32%) (x50,000), (c) SmCo nanoparticles (Sm : 13.54%) (x10,000), (d) SmCo nanoparticles (Sm : 13.54%) (x100,000), (e) SmCo nanoparticle (Sm : 17.80%) (x10,000) and (f) SmCo nanoparticle (Sm : 17.80%) (x50,000).

3-4-1-5. SEM-EDS

SEM-EDS analysis (Fig. 3-38 (a)) was carried out by an electron beams (200 kV) to investigate the contents of the SmCo nanoparticle. EDX data of Fig. 3-38 (a) indicates 2.32% of Sm and 97.68% of cobalt. Fig. 3-38 (b), (c) indicate, in order, the contents of Sm and Co are (b) 13.54%, 86.46% (c) Sm 17.80%, Co 82.20%, respectively. Fig. 3-38 indicates that there is no impurity except the cobalt and samarium components. Washing the product sufficiently is necessary to obtain pure product to remove Na^+ and Cl^- ions.



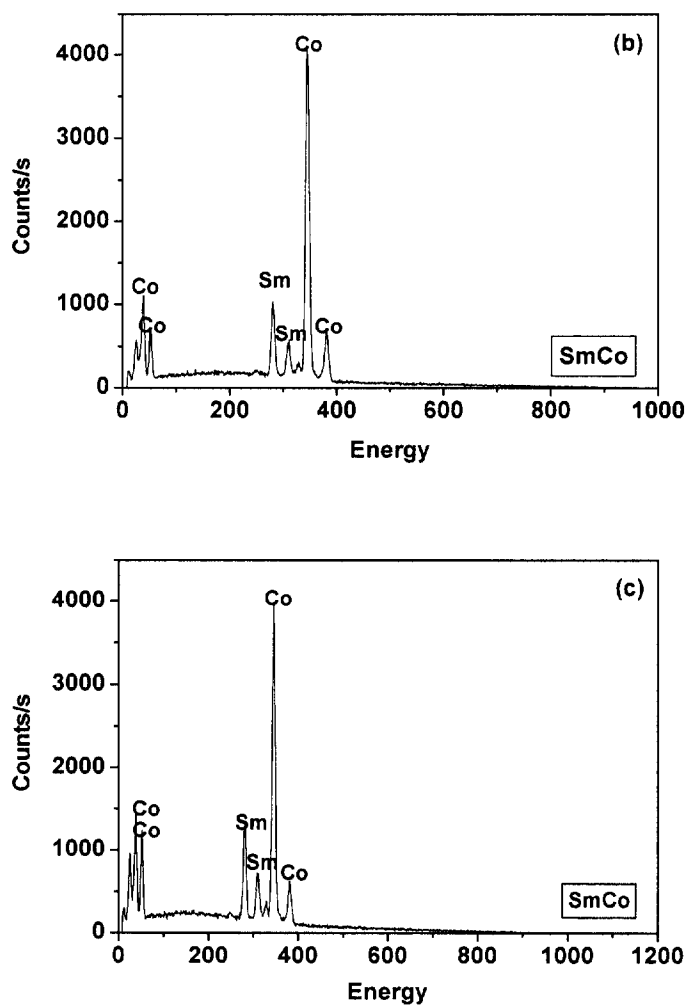
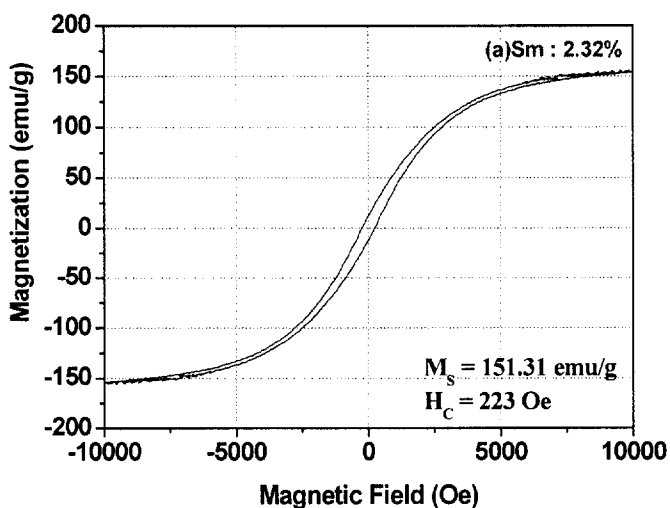


Figure 3-38. SEM-EDS data of SmCo nanoparticles. : (a) SmCo nanoparticles (Sm: 2.32%), (b) SmCo nanoparticles (Sm : 13.54%) and (c) SmCo nanoparticle (Sm : 17.80%).

3-4-1-6. VSM

Fig. 3-39 shows the hysteresis loop of SmCo nanoparticle powders to

characterize magnetic properties at room temperature. The values of saturation magnetization and coercivity are (a) 157.31 emu/g and 223 Oe (Sm:2.32%), (b) 104.7 emu/g, 243 Oe (Sm:13.54%), (c) 78 emu/g , 930 Oe (Sm:17.80%) of SmCo nanoparticles, respectively. The increase of coercivity is resulted from the increase of Sm content of the samples. The salient point of difference between the previous study and ours is to control the size of SmCo nanoparticle and to get nano-sized spherical shape⁵⁵. Generally, the coercivity of the fine particles is found to depend on particle size, and the higher value is realized when the particles have a single domain structure. In this study, the maximum coercivity, 930 Oe, was obtained when the mean diameter of the particles was about 50 nm. The rare earth metal nanoparticle such as SmCo is useful to prepare exchange-coupled magnet through nanocomposition between hard and soft magnetic nanoparticles⁶⁹.



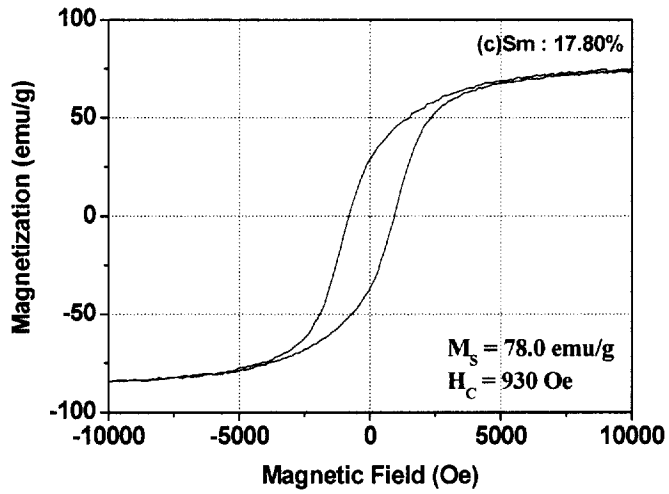
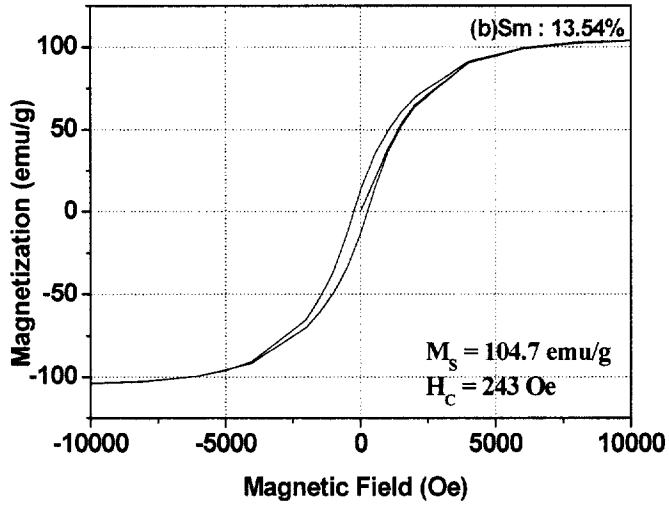


Figure 3-39. The hysteresis loops of SmCo nanoparticle according to the molar ratio of Sm to Co contents : (a) SmCo nanoparticles (Sm: 2.32%), (b) SmCo nanoparticles (Sm : 13.54%) and (c) SmCo nanoparticle (Sm : 17.80%).

3-5. Preparation of $\text{Nd}_2\text{Fe}_{14}\text{B}/\text{Co}$ nanocomposites

3-5-1. Preparation of $\text{Nd}_2\text{Fe}_{14}\text{B}/\text{Co}$ nanocomposites by colloidal process

3-5-1-1. XRD

Fig. 3-40 shows the XRD pattern of the $\text{Nd}_2\text{Fe}_{14}\text{B}/\text{Co}$ nanocomposite samples. The diffraction peak of Co can be indexed to (002) planes of a hexagonal unit cell, corresponding to JCPDS card no. 05-0727. No other peak of impurities is not detected.

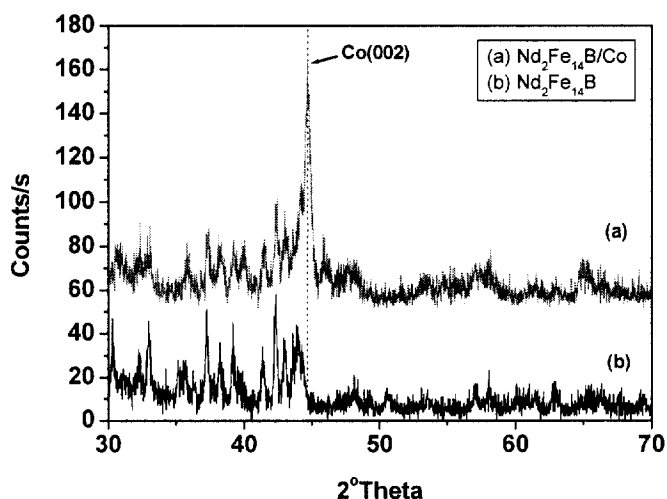
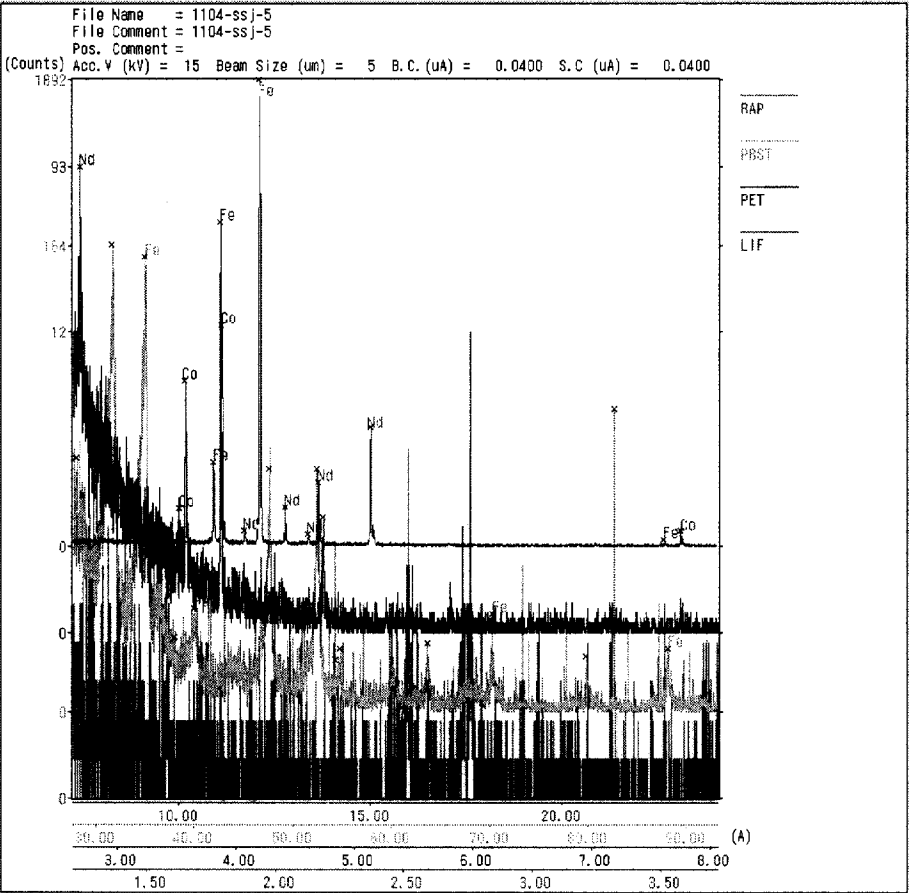


Figure 3-40. (a) X-ray diffractograms of $\text{Nd}_2\text{Fe}_{14}\text{B}$ particles and (b) $\text{Nd}_2\text{Fe}_{14}\text{B}/\text{Co}$ nanocomposites.

3-5-1-2. EPMA

EPMA analysis (Fig. 3-41) was carried out for $\text{Nd}_2\text{Fe}_{14}\text{B}$ particle and

Nd₂Fe₁₄B/Co nanocomposite prepared by colloidal process to obtain contents of our samples. Fig. 3-41 (b) indicates in order the contents of Nd, Fe, B and Co are 10.980, 45.834, 20.971 and 22.214, as atm%. There is no impurity except neodymium, iron, boron and cobalt components. Washing product sufficiently is positively necessary to obtain pure product not including contents of residue ions.



(a)

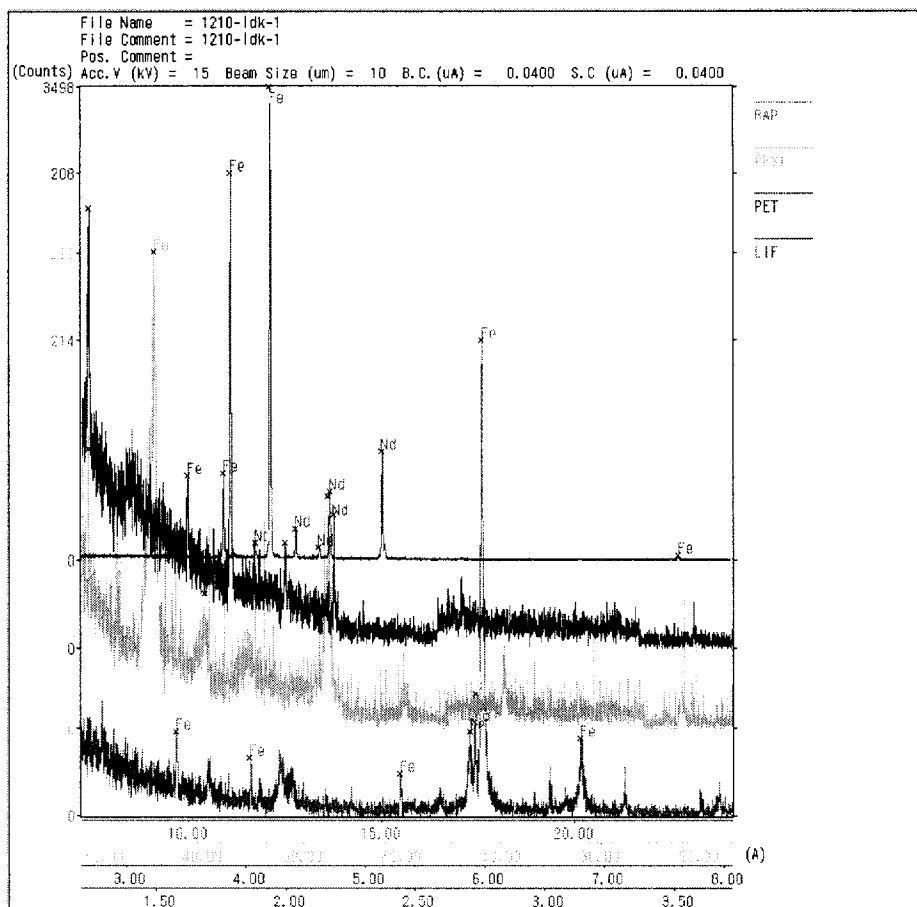
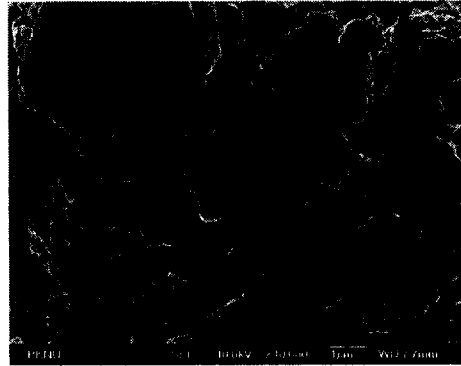


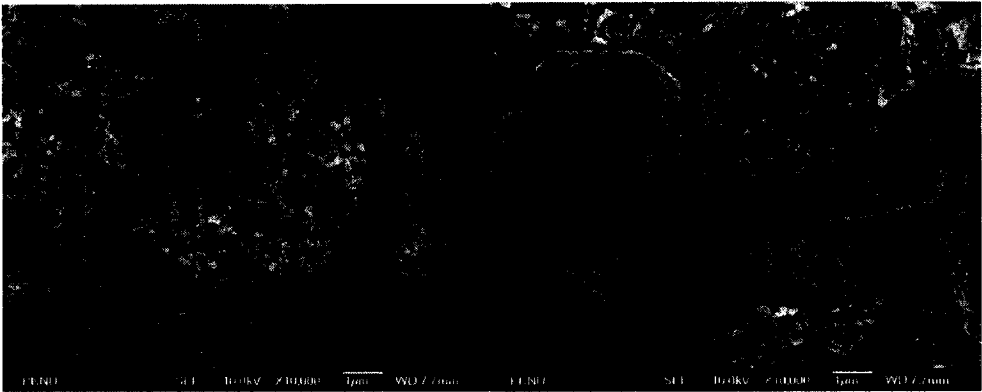
Figure 3-41. (a) EPMA graphs of $\text{Nd}_2\text{Fe}_{14}\text{B}$ particle
(b) $\text{Nd}_2\text{Fe}_{14}\text{B}/\text{Co}$ nanocomposite.

3-5-1-3. FE-SEM

The morphology of the $\text{Nd}_2\text{Fe}_{14}\text{B}$ particle and $\text{Nd}_2\text{Fe}_{14}\text{B}/\text{Co}$ nanocomposite was characterized by FE-SEM images. In Fig 3-42 (b), the excess of Co nanoparticle was added, as compared with Fig. 3-42 (c). In comparison with magnetic properties (Fig. 3-42), the excess of soft phase magnet causes decrease of magnetic properties.



(a)



(b)

(c)

Figure 3-42. (a) FE-SEM images of $\text{Nd}_2\text{Fe}_{14}\text{B}$ (b) $\text{Nd}_2\text{Fe}_{14}\text{B}/\text{Co}$ (Co : 10wt%) (c) $\text{Nd}_2\text{Fe}_{14}\text{B}/\text{Co}$ (Co : 4wt%) nanocomposite

3-5-1-4. VSM

The saturation magnetization (M_s) of magnetic nanoparticle have been determined by using vibrating sample magnetometer with maximum applied field of 15 kOe. Fig. 3-43 shows hysteresis loop of the $\text{Nd}_2\text{Fe}_{14}\text{B}$ particle and core-shell type of $\text{Nd}_2\text{Fe}_{14}\text{B}/\text{Co}$ according to Co content to characterize magnetic properties at room temperature. When Co content was added as 5wt% of $\text{Nd}_2\text{Fe}_{14}\text{B}$ particle, the values of saturation magnetization and

remanence magnetization were increased. That is, the value of BH_{\max} was increased.

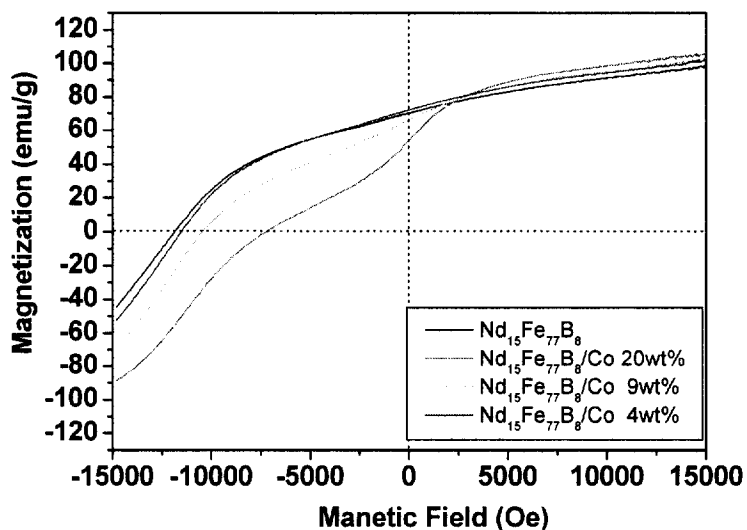


Figure 3-43. The hysteresis loops of $\text{Nd}_2\text{Fe}_{14}\text{B}$ particle and $\text{Nd}_2\text{Fe}_{14}\text{B}/\text{Co}$ nanocomposites according to Co content

4. Conclusion

In this study, the magnetic nanoparticle, Co, FeCo, CoFe₂O₄ were prepared by coprecipitation route and Figlarz's polyol process. Co and FeCo nanoparticles were studied according to different preparation methods and the effect of surfactant and precursors to control particle size. The preparation of magnetic material nanoparticles with controlled size has been studied. It was easy to control particle size with polyol method. The saturation magnetization was compared in compliance with different preparation process. The SmCo and Co nanoparticles were synthesized by thermal decomposition method that is a new solventless synthesis by thermolysis of metal-oleate complex under low pressure (0.8 torr). Those magnetic nanoparticles were obtained as uniform size of 40 nm, more or less. Moreover, the increase in SmCo particle size is quite obvious with increasing Sm contents due to disposition of SmCo alloy to form hexagonal shape. The SmCo nanoparticle that has high Sm contents (17.80%) shows the highest coercivity of 930 Oe with saturation magnetization of 78 emu/g. The core shell type of Nd₂Fe₁₄B/Co nanocomposite was prepared by colloidal process according to the weight% of Co to Nd₂Fe₁₄B.

5. References

1. Bagrets, N.; Perov, N.; Bagrets, A.; Lermontov, A.; Pankina, G.; Chernavskii, P., *J. Magn. Magn. Mater.* **2004**, 272-276, 1565.
2. Kodama, R. H., *J. Magn. Magn. Mater.* **1999**, 200, 359.
3. Viau, G.; Fievet-Vincent, F.; Fievet, F., *Solid State Ionics* **1989**, 32/33, 198.
4. Ferrier, G. G.; Benzins, A. R.; Davey, N. M., *Platinum Matels Rev.* **1985**, 29, 175.
5. Smith, T. W.; Wychick, *J. Phys. Chem.* **1980**, 84, 1621.
6. Hahn, H.; Averbach, R. S., *J. Appl. Phys.* **1990**, 67, 1113.
7. Klabunde, K. J.; Zhang, D.; Glavee, G. N.; Sorensen, C. M., *Chem. Mater.* **1994**, 6, 784.
8. Suslick, K. S.; Fang, M.; Hyeon, T., *J. Am. Chem. Soc.* **1996**, 118, 11960.
9. Bönemann, H.; Brijoux, W.; Brinkmann, R.; Joussen, T., *Angew. Chem., Int. Ed. Engl.* **1990**, 29, 273.
10. Tsai, K.-L.; Dye, J. L., *J. Am. Chem. Soc.* **1991**, 113, 1650.
11. Bensebaa, F.; Zavaliche, F.; L'Ecuyer, P.; Cochrane, R. W.; Veres, T., *J. Colloid and Interface Science.* **2004**, 277, 104.
12. Dong, X.L.; Choi, C. J.; Kim, B. K., *Scripta Materialia.* **2002**, 47, 857.
13. Park, S. J.; Kim, S.; Lee, S.; Khim, Z.G.; Charand, K.; Hyeon, T., *J. Am. Chem. Soc.* **2000**, 122, 8581.
14. Sun, S.; Murray, C. B., *J. Appl. Phys.* **1999**, 85, 4325.
15. Petit, C.; Taleb, A.; Pileni, M.P., *J. Phys. Chem. B.* **1999**, 103, 1805.
16. Puentes, V. F.; Krishnan, K. M.; Alivisatos, A. P., *Science.* **2001**, 291, 2115.
17. Sun, S.; Zeng, H., *J. Am. Chem. Soc.* **2002**, 124, 8204.
18. Ayyappan, S.; Subbanna, G. N.; Srinivasa Gopalan, R.; Rao, C. N. R.

- Solid State Ionics*. **1996**, 84, 271.
19. Viau. G.; Toneguzzo, P.; Acher, O.; Fievet-Vincent, F.; Fievet. F., *Scripta Mater.* **2001**, 44, 2263.
 20. Hegde, M. S.; Larcher. D.; Dupont, L.; Beaudion, B.; Tekaiia-Elhsissen, K.; Tarascon, J.-M., *Solid State Ionics*. **1997**, 93, 33.
 21. Viau. G.; Ravel. F.; Acher, O.; Fievet-Vincent, F.; Fievet. F., *J. Magn. Magn. Mater.* **1995**, 140-144, 377.
 22. Hinotsu, E. T.; Jeyadevan, B.; Chinnasamy, C.N.; Shinoda, K.; Tohji, K., *J. Appl. Phys.* **2004**, 95, 7477.
 23. Lin, J. H.; Liu, S. F.; Qian, X. L.; Bayi, J. M.; Su, M. Z., *J. Alloys Compds.* **1996**, 238, 113.
 24. Chinnasamy, C.N.; Jeyadevan, B.; Perales-Perez, O.; Shinoda, K.; Tohji, K.; Kasuya, A., *IEEE Trans. Magn.* **2002**, 38, 264.
 25. Leccabue, F.; Salviati, G.; Almodovar, N. S.; Albanese, G.; Leo, G., *IEEE Trans. Magn.* **1988**, 300 1850.
 26. Wu, K. T.; Kuo, P.C.; Yao, Y.D.; Tsai, E. H., *IEEE Trans. Magn.* **2001**, 37, 2651.
 27. Micheli, A. L., *IEEE Trans. Magn.* **1970**, 6, 606.
 28. Yu, R. H.; Basu, S.; Zhang, Y.; Parvizi-Majidi, A.; Xiao, J. Q., *J. Appl. Phys.* **1999**, 85, 6655.
 29. Li, L., *J. Appl. Phys.* **1996**, 79, 4578.
 30. Corrias, A.; Ennas, G.; Licheri, G.; Marongiu, G.; Paschina, G., *Chem. Mater.* **1990**, 2, 363.
 31. Lin, J.H.; Liu, S.F.; Cheng, Q.M.; Qian, X.L.; Yang, L.Q.; Su, M.Z., *J. Alloys Compds.* **1997**, 249, 237.
 32. Silvert, P. Y.; Tekaiia-Elhsissen, K., *Solid State Ionics* **1995**, 82, 53.
 33. Viau, G.; Pierrard, A.; Fievet-vincent, F.; Fievet, F., *IEEE Trans. Magn.* **1999**, 35, 3469.

34. Viau, G.; Fievet-Vincent, F. ; Fievet, F., *J. Mater. Chem.* **1996**, 6, 1047.
35. Sasaki, Y. ; Tsuboi, S. ; Kasajima, N. ; Kitahata, S. ; Kishimoto, M., *IEEE Trans. Magn.* **2001**, 37, 2204.
36. Wang, Y.; Toshima, N.; J. Phys. Chem. B. **1997**, 101, 5301.
37. Kneller, E.F.; Hawig, R., *IEEE Trans. Magn.* **1991**, 27, 3588.
38. Schrefl, T.; Fidler, J.; Kronmüller, H., *Phys. Rev. B.* **1994**, 49, 6100.
39. Ding, J.; McCormick, P. G.; Street, R., *J. Magn. Magn. Mater.* **1993**, 124, 1.
40. Cui, B.C.; Sun, X. K.; Liu, W.; Zhang, Z.D.; Geng, D.Y.; Zhao, X. G., *J. Appl. Phys.* **2000**, 87, 5335.
41. Zhang, X.Z.; Guan, Y.; Yang, L.; Zhang, J.W., *Appl. Phys. Lett.* **2001**, 79, 2426.
42. Liu, J.P.; Sellmyer, D. J., *J. Appl. Phys.* **1998**, 83, 6608.
43. Cui, B.C.; Sun, X.K.; Liu, W.; Zhang, Z.D.; Geng, D.Y.; Zhao, X.G., *J. Appl. Phys.* **2000**, 87, 5335.
44. You, C.Y.; Sun, X.K.; Liu, W.; Cui, B.Z.; Zhao, X.G.; Geng, D.Y.; Zhang, Z.D., *J. Phys. D: Appl. Phys.* 35 (2002) 943.
45. Cao, G., *Nanostructures and Nanomaterials, Synthesis, Properties and Application.* **2004**, 1-4.
46. Poole, C. P.; Owens, F. J., *Introduction of Nanotechnology*, **2003**, 165.
47. McCurrie, R. A., *Ferromagnetic Materials, Structure and Properties.* **1994**, 1-2.
48. Goldman, A., *Handbook of Modern Ferromagnetic Materials.* **1999**, 4-15.
49. Zeng, H.; Li, J.; Liu, J. P.; Wang, Z. L.; Sun, S. *Nature.* **2002**, 420, 395.
50. Skomski, R.; Coey, J. M. D. *Phys. Rev. B* **1993**, 48, 15812.

51. Kneller, E. E.; Hawig, R. *IEEE Trans. Mag.* **1991**, 27, 3588.
52. Liu, J. P. in *Nanophase and Nanostructured Materials* Vol. 3 (Wang, Z. L.; Liu, Y.; Zhang, Z., Ed.) 230-267 (Tsinghua Univ. Press/Kluwer, 2002)
53. Figlarz, M.; Ducamp-Sanguesa, C.; Fievet, F.; Lagier, J.P., *Adv. Metall. Particul. Mater.* **1992**, 1, 179.
54. Ducamp-Sanguesa, C.; Herrera-Urbina, R.; Figlarz, M., *Solid State Ionics.* **1993**, 63-65, 25.
55. Ducamp-Sanguesa, C. ; Herrera-Urbina, R. ; Figlarz, M., *J. Solid State Chem.* **1992**, 100, 272.
56. Figlarz, M. ; Fievet, F. ; Lagier, J.P., *MRS Intern. Meeting on Advanced Materials* **1989**, to be published.
57. Fievet, F.; Lagier, J.P. ; Figlarz, M., *MRS Bull.* **1989**.
58. Fievet, F.; Lagier, J.P.; Figlarz, M., *M.R.S. Bull.* **1989**, 14, 29.
59. Viau. G.; Fievet-Vincent, F.; Fievet. F., *Solid State Ionics.* **1996**, 84, 259.
60. Shen, J.; Li, Z.; Yan, Q.; Chen, Y., *J.Phys. Chem.* **1993**, 97, 8504.
61. Levy, A.; Brown, J.B.; Lyons, C. J. *Ind. Eng. Chem.* **1960**, 52, 211.
62. Yang, H. T.; Su, Y. K.; Shen, C. M.; Yang, T. Z.; Gao, H., *J. Surface and Interface Analysis*, **2004**, 36, 155.
63. Hegde, M. S.; Larcher, D.; Dupont, L.; Beaudoin, B.; Tekaiia- Elhsissen, K.; Tarascon, J.-M., *Solid State Ionics*, **1997**, 93, 33.
64. Schobinger, D.; Gutfleisch, O.; Hinz, D.; Mller, K.-H.; Schultz, L.; Martinek, G., *J. Magn. Magn. Mater.* **2002**. 242, 1347.
65. Tang, W.; Zhang, Y.; Goll, D.; Hadjipanayis, G.C.; Kronmüller, H., *J. Magn. Magn. Mater.*, **2001**, 226-230, 1365.
66. Wang, J. Y.; Ghantasala, M. K.; Sood, D. K.; Evans, P., *J. Thin Solid Films.* **2005**, 489, 192.

67. Handstein, A.; Kubis, M.; Gutfleisch, O.; Gebel B.; Müller, K. -H., *J. Magn. Magn. Mater.*, **1999**, 192, 73.
68. Campos, M. F.; Rios P. R., *J. Alloys and Compds.* **2004**, 377, 12.
69. Fullerton, E. E.; Jiang, J. S.; Sowers, C. H., Pearson, J. E.; Bader, S. D., *Appl. Phys. Lett.* **1997**, 72, 380.

6. Korean abstract

본 연구에서 자성체 연자성 나노입자 Co , FeCo , CoFe_2O_4 는 열분해법, 화학적 환원과정(공침법)을 통해 합성되었다. 제조되어진 자성체 나노입자는 다른 합성방법, 용매효과와 사이즈 조절을 위해 쓰여진 계면활성제의 효과에 대해 연구하였다. 또한 Co , SmCo 나노입자는 Co^{2+} -oleate₂, Sm^{2+} -oleate₂와 Co^{2+} -oleate₂ 복합체를 pyrex 튜브를 이용하여 400 °C 고온, 0.8 torr의 낮은 압력에서 열분해하여 합성하였다. 볼밀법으로 제조한 경자성체 $\text{Nd}_2\text{Fe}_{14}\text{B}$ 는 core-shell 형태의 나노복합체로 합성하여 교환상호작용을 통한 자기적 특성을 연구하였다. 제조되어진 나노입자들과 나노복합체의 포화자화값과 보자력값은 VSM과 SQUID를 이용하여 나노입자들의 성분예 따라 비교분석하였다. 입자의 형태나 사이즈는 전자현미경으로 분석하였고, SEM-EDS로 구성성분을 XRD로 반폭치와 결정면을 분석하였다.